

RESEARCH ARTICLE

10.1029/2018JE005664

Special Section:

Planetary Mapping: Methods,
Tools for Scientific Analysis and
Exploration

This article is a companion to Séjourné
et al. (2018), <https://doi.org/10.1029/2018JE005665>; Ramsdale et al. (2018),
<https://doi.org/10.1029/2018JE005663>.

Key Points:

- A grid-mapping approach is demonstrated to be an effective technique to map small-scale landforms in Acidalia Planitia
- LDM begins to occur north of 44 degree N in Acidalia Planitia, a transition that is at a higher latitude than in Utopia and Arcadia Planitiae
- Irregular-shaped pits on equator-facing scarps suggest an energetic release of volatiles (H₂O, CO₂, CH₄)

Supporting Information:

- Supporting Information S1
- Supporting Information S2
- Supporting Information S3

Correspondence to:

C. Orgel,
orgel.csilla@fu-berlin.de

Citation:

Orgel, C., Hauber, E., van Gasselt, S., Reiss, D., Johnsson, A., Ramsdale, J. D., et al. (2019). Grid mapping the northern plains of Mars: A new overview of recent water- and ice-related landforms in Acidalia Planitia. *Journal of Geophysical Research: Planets*, 124, 454–482. <https://doi.org/10.1029/2018JE005664>













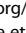
Received 28 APR 2018

Accepted 8 AUG 2018

Accepted article online 13 SEP 2018

Published online 21 FEB 2019

Grid Mapping the Northern Plains of Mars: A New Overview of Recent Water- and Ice-Related Landforms in Acidalia Planitia

Csilla Orgel^{1,2} , Ernst Hauber² , Stephan van Gasselt^{1,3} , Dennis Reiss⁴, Andreas Johnsson⁵, Jason D. Ramsdale⁶ , Isaac Smith⁷ , Zuzanna M. Swirad⁸ , Antoine Séjourné⁹ , Jack T. Wilson¹⁰ , Matthew R. Balme⁶ , Susan J. Conway^{6,11} , Francois Costard⁹ , Vince R. Eke¹², Colman Gallagher^{13,14} , Ákos Kereszturi¹⁵, Anna Łosiak^{16,17}, Richard J. Massey¹², Thomas Platz^{1,18} , James A. Skinner¹⁹, and Luis F. A. Teodoro²⁰

¹Institute of Geological Sciences, Planetary Sciences and Remote Sensing, Freie Universität Berlin, Germany, ²DLR-Institut für Planetenforschung, Berlin Adlershof, Germany, ³Department of Land Economics, National Chengchi University, Taipei, Taiwan, ⁴Institut für Planetologie, Westfälische Wilhelms-Universität Münster, Germany, ⁵Department of Earth Sciences, University of Gothenburg, Sweden, ⁶Department of Physical Sciences, The Open University, Milton Keynes, UK, ⁷Institute for Geophysics, University of Texas, Austin, TX, USA, ⁸Department of Geography, Durham University, Durham, UK, ⁹GEOPS, Université Paris-Sud, CNRS, Université Paris-Saclay, Orsay, France, ¹⁰The Johns Hopkins Applied Physics Laboratory, Laurel, MD, USA, ¹¹Laboratoire de Planétologie et Géodynamique-UMR CNRS 6112, Nantes, France, ¹²Institute for Computational Cosmology, Department of Physics, Durham University, Durham, UK, ¹³UCD School of Geography, University College Dublin, Ireland, ¹⁴UCD Earth Institute, University College Dublin, Ireland, ¹⁵Konkoly Observatory, Research Centre for Astronomy and Earth Sciences, Hungarian Academy of Sciences, Budapest, Hungary, ¹⁶Institute of Geological Sciences, Polish Academy of Sciences, Warsaw, Poland, ¹⁷wildFIRE Lab, University of Exeter, UK, ¹⁸Max Planck Institut für Sonnensystemforschung, Göttingen, Germany, ¹⁹USGS Astrogeology Science Center, Flagstaff, AZ, USA, ²⁰BAER, Planetary Systems Branch, Space Science and Astrobiology Division, NASA Ames Research Center, Moffett Field, CA, USA

Abstract We used a grid-mapping technique to analyze the distribution of 13 water- and ice-related landforms in Acidalia Planitia as part of a joint effort to study the three main basins in the northern lowlands of Mars, that is, Acidalia, Utopia, and Arcadia Planitiae. The landforms were mapped at full Context Camera resolution along a 300-km-wide strip from 20°N to 84°N. We identified four landform assemblages: (1) Geologically recent polar cap (massive ice), which superposes the latitude-dependent mantle (LDM) (LA1); (2) ice-related landforms, such as LDM, textured terrain, small-scale polygons, scalloped terrain, large-scale viscous flow features, and gullies, which have an overlapping distribution (LA2); (3) surface features possibly related to water and subsurface sediment mobilization (LA3; kilometer-scale polygons, large pitted mounds, small pitted mounds, thumbprint terrain); and (4) irregularly shaped pits with raised rims on equator-facing slopes. Pits are likely the result of an energetic release of volatiles (H₂O, CO₂, and CH₄), rather than impact-, volcanism-, or wind-related processes. LDM occurs ubiquitously from 44°N to 78°N in Acidalia Planitia. Various observations suggest an origin of air fall deposition of LDM, which contains less ice in the uppermost tens of meters in Acidalia Planitia than in Arcadia and Utopia Planitiae. However, LDM may be thicker and more extended in the past in Acidalia Planitia. The transition between LDM-free terrain and LDM is situated further north than in Utopia and Arcadia Planitiae, suggesting different past and/or present climatic conditions among the main basins in the northern lowlands.

Plain Language Summary We studied water and ice-related landforms in the Acidalia Planitia, Mars. We used a new approach, a grid system of 20 × 20-km cells, along a 300-km-wide strip (east-west) from latitude 20°N to 84°N (south-north). This work is a joint effort to study three major basins in the northern plains: Acidalia, Utopia, and Arcadia Planitiae. We conducted a regional mapping of specific landforms at 6 m/pixel resolution data and compared the results to different data products, such as geological maps, topography, radar, and climatic models. We proved that latitude-dependent mantle occurs from 44°N to 78°N in Acidalia Planitia and has an air fall origin related to past climatic cycles. These deposits are composed of mixture of fine-grained ice and dust. The distribution of this landform extends further south in Utopia and Arcadia Planitiae suggesting different past/present climatic conditions in the northern lowlands.

1. Introduction

1.1. Recent Landforms in the Northern Plains on Mars: An Overview

Although the surface of the northern lowlands appears smooth and flat at kilometer scale (Kreslavsky & Head, 2000), many small landforms are visible at smaller scale. Of special interest are landforms that have long been interpreted as results of the presence and action of water and/or ice (e.g., Kargel et al., 1995), a notion that was supported when high-resolution images became available and provided evidence for the aggradation and degradation of materials in a permafrost context (e.g., Morgenstern et al., 2007; Séjourné et al., 2012). Moreover, the lowlands cover the northern part of the bihemispheric latitude belt of $\sim 30^\circ$ to $\sim 60^\circ$, which hosts a variety of possible periglacial and glacial landforms such as thermal contraction cracks, gullies, and viscous flow features, VFF (e.g., Harrison et al., 2015; Hubbard et al., 2014; Levy et al., 2010; Milliken et al., 2003). These and other landforms such as a layered latitude-dependent mantle (LDM; Kostama et al., 2006; Kreslavsky & Head, 2002a; Mustard et al., 2001) may represent a morphological record of recent ice ages (Head et al., 2003). Moreover, a growing number of observations suggests the existence of significant volumes of subsurface excess ice in the northern lowlands (Bramson et al., 2015; Byrne et al., 2009; Kadish et al., 2009; Pathare et al., 2018; Stuurman et al., 2016; Viola et al., 2015, 2017), some of which seem to be exposed at cliffs (Dundas, et al., 2018). As such ice reservoirs are not in equilibrium with current atmospheric conditions, it has been suggested that the ice was precipitated during recent episodes of different climatic conditions (e.g., Head et al., 2003, and further references therein; Dundas et al., 2014; Bramson et al., 2017) forced by orbital and spin-axis variations (e.g., Forget et al., 2017; Laskar et al., 2004).

The geographical distribution of water- and/or ice-related landforms can provide important constraints on their formation mechanism and the past Martian climate and its evolution. While the populations of some of the landforms that are relevant for the recent volatile and climate history of Mars have been localized (e.g., Balme et al., 2006; Dickson et al., 2007; Harrison et al., 2015; Hubbard et al., 2014; Kadish et al., 2009; Levy et al., 2010), a comprehensive mapping of all of them over the entire lowlands is still missing. However, given the small scale of many such landforms and surface textures, their large number and overlapping relationship over the vast expanse of the northern lowlands, it appears inefficient to map them individually and represent the results in a traditional map. Instead, it was the objective of an International Space Science Institute team to map three north-south traverses across the major lowland basins (Arcadia, Utopia, and Acidalia Planitiae; Figure 1) and focus on possibly ice-related landforms (Table 1). We used a recently developed grid-mapping technique (Ramsdale et al., 2017), which enables effective and fast mapping of small-scale landforms over large areas. This technique (described in detail below) was successfully applied to the Hellas impact basin (Voelker et al., 2017) and results in a consistent and comparable database of landform locations, which can subsequently be statistically interrogated for different spatial relationships. We report on the results of the grid mapping as well as any serendipitous science observations in three separate studies covering Acidalia Planitia (this study), Arcadia Planitia (Ramsdale et al., 2018), and Utopia Planitia (Séjourné et al., 2018). In the following, we provide first an overview on the context and the geology of Acidalia Planitia (sections 1.2). We then describe the applied grid-mapping techniques (section 2), present the mapping results (section 3), and the mutual spatial relations of landforms as well as their relation to independent parameters such as topography or geology (section 4), and finally discuss the implications of our findings (section 5).

1.2. Geology

In the southern part of the study area, the oldest Noachian geologic units are the highly cratered Noachis Terra unit (Nn), Crater (AHC) and Crater floor (AHCf) units in the dichotomy boundary, and the Hesperian fluvial material of Chryse Planitia 1 (HNCc1) and 2 (HCc2) units (Tanaka et al., 2014). Further north, the Acidalia Mensae/Acidalia Colles region is located and exposes the Noachis Terra unit and the mass-wasting talus deposits of Nepenthes Mensae (HNn) unit (Tanaka et al., 2014; Figure 13n). The Acidalia Colles form a topographically high plateau a few hundred meters above the northern plains and is characterized by a relatively smooth surface, which represents mass-wasting, sedimentary, and volcanic origins (Tanaka et al., 2014). It is overlaid by the most extensive geologic unit in the northern lowlands, the so-called Late-Hesperian/Early-Amazonian Vastitas Borealis Formation (VBF) with the interior (ABvi) and marginal (ABvm) units (Figure 13n). The VBF is a sedimentary veneer that formed as the residue of outflow channel deposits and overlies the Hesperian ridged volcanic plains material (Rice & Edgett, 1997). The VBF has a characteristic

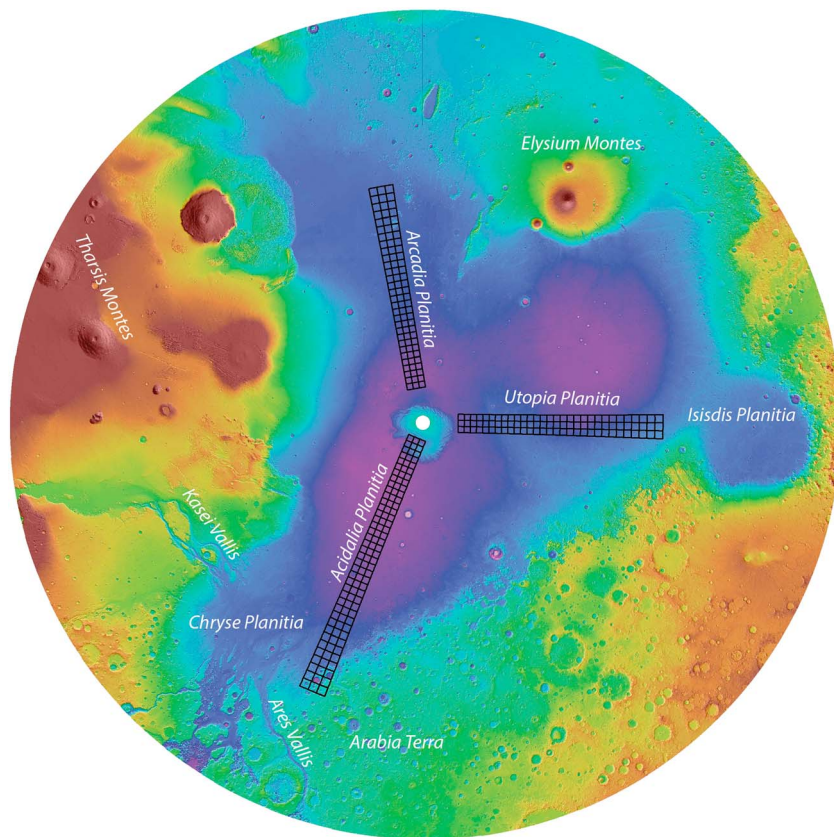


Figure 1. Overview map of the three main basins of the northern lowlands: Acidalia (this study), Utopia (Séjourné et al., 2018), and Arcadia Planitiae (Ramsdale et al., 2018).

surface roughness at 3-km scale and an estimated minimum thickness of 100 m (Kreslavsky & Head, 2000, 2002b). Werner et al. (2011) proposed a formation age for VBF between 3.75 and 3.4 Ga. Ivanov et al. (2014, 2015) estimated an absolute model age of 3.61 (+0.05/−0.08) Ga for Acidalia Planitia and a similar age of 3.57 ± 0.02 Ga for the surface units of Utopia Planitia that is in good agreement with the existence of a hypothesized Late-Hesperian ocean (Kreslavsky & Head, 2000, 2002b).

2. Data and Methods

2.1. Study Area

The study area in Acidalia Planitia (Figure 1) is a 300-km-wide strip extending from latitude 20°N to 84°N, centered on longitude 22.5°W. The selection of the location of the strip primarily maximized the availability of CTX (Context Camera) 6 m/pixel images in early 2014. We used CTX as it has nearly global coverage and spatial resolution that is sufficient to resolve landforms associated with ice at or close to the surface.

2.2. Data

2.2.1. Imaging

The data set best suited to serve as a base map for our approach was acquired through the CTX instrument on the MRO (Mars Reconnaissance Orbiter) spacecraft (Malin et al., 2007). It offers both good contiguous spatial coverage and a relatively high spatial resolution. The images were obtained from the Planetary Data System archive and processed with the Integrated Software for Imaging Spectrometers software developed for planetary data processing by USGS in Flagstaff. After processing we compiled a mosaic with a resolution of 6 m/pixel.

We also used images from the MRO High-Resolution Imaging Science Experiment (HiRISE, 25 or 50 cm/pixel in map projection; McEwen et al., 2010) for detailed inspection where available.

Table 1
Landform Classes Used in The Geomorphological Grid Mapping

#	Name	Brief description	Reference	Putative origin
1	Latitude dependent mantle (LDM)	Deposits that mantle the underlying terrain, resulting in a smoothed-looking topography	Kreslavsky and Head (2002a), Mustard et al. (2001), Kostama et al. (2006)	Formation related to ice and dust precipitation from the atmosphere.
2	Textured terrain	Pits and knobs, basketball-, brain terrain, wrinkled pattern	Mangold (2005), Kostama et al. (2006), Levy et al. (2009b)	Dissection/modification features of the LDM
3	Small-scale polygon	Orthogonal polygon networks that are tens to hundreds of meters in size on intercrater plains and on crater floors	Seibert and Kargel (2001), Mangold (2005), Marchant and Head III (2007), Levy et al. (2009a, 2010), Soare, Conway, and Dohm (2014)	Potential origin related to sand-wedge polygons or sublimation-type polygons
4	Scalloped terrain	Isolated or coalesced shallow, rimless depressions exhibiting steeper poleward facing scarps	Costard and Kargel (1995), Morgenstern et al. (2007), Soare et al. (2008, 2011), Lefort et al. (2009, 2010), Ulrich et al. (2010), Zanetti et al. (2010), Séjourné et al. (2011), Dundas, Byrne, and McEwen (2015)	Degradation of subsurface ice
5	Gullies	Erosional landform, young age (10^5 to 10^6 years), length up to a few kilometers, characterized by a head alcove, incised channel, and debris apron	Malin and Edgett (2000), Costard et al. (2002), Christensen (2003), Treiman (2003), Bridges and Lackner (2006), Dickson et al. (2007), Heldmann et al. (2007); Pelletier et al. (2008), Kneissl et al. (2010), Canzler (2014), Decker (2015), Harrison et al. (2015), Dundas, Diniega, and McEwen (2015)	Origin debated; indicative either of liquid water/debris flows or of dry mass wasting processes involving CO ₂ frost/ice.
6	Pits	50–150 m in diameter shallow pits with raised, wavy rims occur on equator-facing slopes in craters and on ridges		Raised rims might indicate “explosive” mechanism, rather than sublimation processes
7	Viscous flow features (VFF)	All mesoscale landforms indicative of creep of ice and debris	Lucchitta (1981), Milliken et al. (2003), Head III, Marchant, et al. (2006), Head III, Nahm, et al. (2006), van Gasselt et al. (2010), Hubbard et al. (2014)	Creep of mixture of ice and debris
8	Km-scale polygons	Delineating troughs with an average depths of ~30 m and spacing of 5 to 10 km	Hiesinger and Head (2000), Oehler and Allen (2010), Berndt et al. (2012), Moscardelli et al. (2012), Allen et al. (2013), Orgel et al. (2015)	Potential origins related to fluid expulsion structures in terrestrial submarine environment or elastic rebound after removing water or ice from the ground
9	Large pitted mounds (LPM)	From hundreds of meters to km-scale dome or pancake-like features, commonly with a summital pit or crater	Farrand et al. (2005), McGowan (2009), Skinner and Mazzini (2009), Oehler and Allen (2010), Allen et al. (2013), Salvatore and Christensen (2014), Orgel et al. (2015)	Origin of rapid sedimentation of fluid-rich sediment, dewatering, and fluid expulsion processes (mud volcanism)
10	Small pitted mounds (SPM)	Similar to large pitted mounds, but in smaller size (average basal diameter: 170 m) and generally forms in clusters	Farrand et al. (2005), Orgel et al. (2015)	Might have formed by the vaporization of volatiles of shallowly buried clathrates or fluid expulsion processes (mud volcanism)
11	Thumbprint terrain (TPT)	Uniformly sized cones with average basal diameter of 455 m and multiple summit pits usually arranged in curvilinear chains of mounds or ridges or cones	Plescia (1980), Grizzaffi and Schultz (1989), Lokwood et al. (1992), Davis and Tanaka (1995), Bridges et al. (2003), Bruno et al. (2004), Farrand et al. (2005), Ghent et al. (2012), Orgel et al. (2015), Gallagher et al. (2018)	Multiple proposed origin: cinder cones, sublimation or lacustrine features, mud volcanoes, tuff cones, phreatomagmatic features, devolatilized pyroclastic flows
12	Massive ice	Exposed surface ice		Part of the northern polar cap
13	Bedrock	Lithified rock surface		No sediment coverage or landforms

Note. See Figures 4–11 for image examples of each landform.

2.2.2. Topography

The only data set that provides topographic information across the entire mapping traverse is the gridded MOLA (Mars Orbiter Laser Altimeter) DEM (Digital Elevation Model), with a cell size of 463 m (Figure 2a; Smith et al., 2001). It is interpolated from MOLA profiles, which have individual shot spacing along-track spacing of 300 m. These profiles are aligned in an approximately north-south direction along the near polar orbit of the MGS spacecraft (Albee et al., 1998) and were used for detailed topographic analysis at selected locations. We also used data derived from the gridded MOLA DEM, such as slope maps and roughness maps at different base lengths. A kilometer-scale surface roughness map at 0.6-, 2.4-, and 9.2-km scale derived

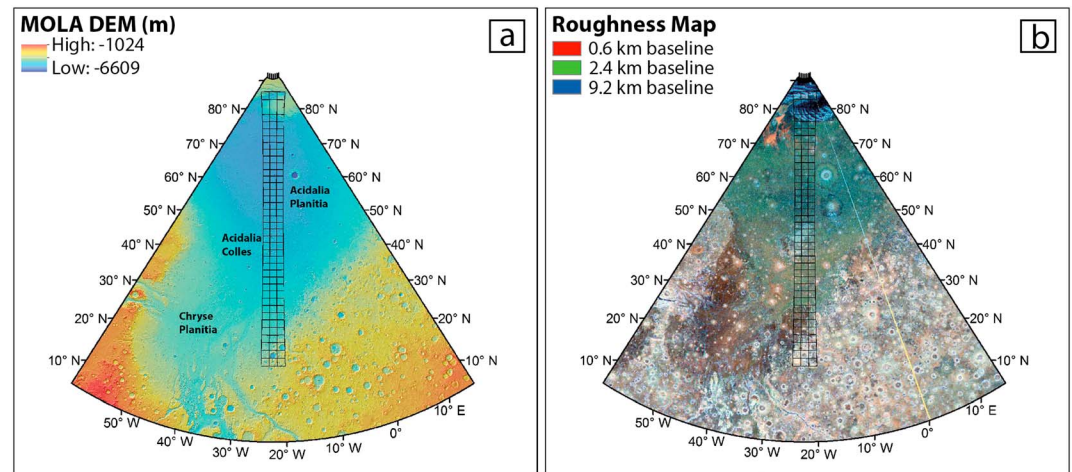


Figure 2. Acidalia wide area maps in Lambertian conformal conic projection with the grid strip. (a) Topography derived from MOLA DEM, (b) roughness composite map derived from Kreslavsky and Head (2000). MOLA = Mars Orbiter Laser Altimeter; DEM = Digital Elevation Model.

from MOLA profiles was used from Kreslavsky and Head (2000; Figure 2b). It is important to note that slopes referred to in this study were derived from gridded MOLA DEM, that is, measured over base lengths of several hundred meters and can be considered regional slopes. Locally, however, much steeper slopes exist in the mapping area.

2.2.3. SHALLOW RADAR

To correlate the subsurface structures with the geomorphological observations, we analyzed the MRO SHALLOW RADAR (MRO SHARAD, vertical: 10 m/pixel, horizontal: 300–1,000 m/pixel, along track, 3,000–6,000 m/pixel, cross-track) data (Seu et al., 2004). We analyzed 157 observations from the shallow radar (SHARAD) instrument that cross the Acidalia Planitia swath (Figure 15). Radar profiles (radargram + simulation) were interpreted in several steps. First, a comparison with a simulated radargram, based on topographic data from the MOLA (Smith et al., 2001) was completed. Simulated radargrams are designed to predict where reflections that originate on the surface, both from nadir and to the side, will lie on the collected radargram. Often, surface side reflections appear beneath the surface due to their longer time delay than the nadir point. These reflections, or clutter, must be distinguished from true subsurface reflections. Therefore, where clutter is predicted and matches a subsurface interface, we do not interpret a subsurface reflection. However, when clutter is not predicted for a location but a reflection appears, we interpret that to indicate a subsurface interface and mark it in the grid.

The second step is to distinguish sidelobes. Sidelobes are an artifact of radar processing deconvolution that occur just below the surface echo. They parallel the surface reflection and are always at a lower intensity. Reflections that are determined to be neither clutter nor sidelobes were considered to be subsurface interfaces.

Radar reflections represent an interface between contrasting materials and may come from many sources: air-regolith; regolith-ice; ice-basement. In this grid-mapping survey we search only for detection interfaces and do not measure the dielectric properties of the materials that create the reflection. Thus, composition of the material causing the reflection is not constrained. The spatial relationships are recorded for each orbital/observation ground track. All detections were then recorded and projected into map view while looking for spatial correlations. The methods employed here are described in more detail in Smith and Holt (2015).

2.2.4. Other Map Products

Several other data sets and map products were used for comparison to our results. A Water Equivalent Hydrogen (WEH) map compiled from the Mars Odyssey Neutron Spectrometer (MONS) data (Wilson et al., 2018) and models of ground ice depth and ice stability at different obliquity (Chamberlain & Boynton, 2007; Mellon et al., 2004; Mellon & Jakosky, 1995) were compared to the distribution of landforms, especially which were suspected to have an origin of ice-related processes (e.g., LDM, textured terrain, scalloped terrains, small-scale polygons, and gullies).

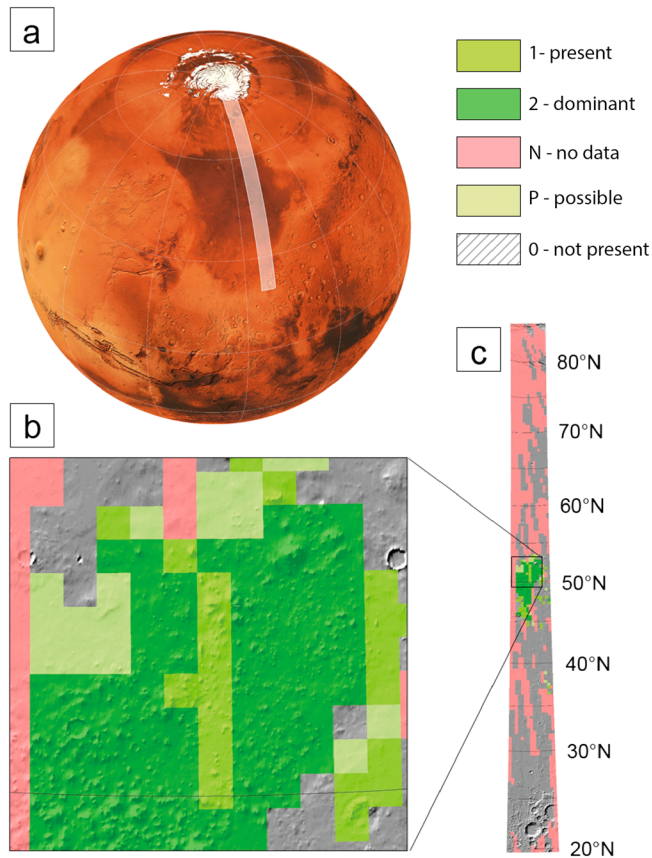


Figure 3. Schematic illustration of the grid-mapping technique. (a) Global view of the complete mapping strip. (b) Exemplary result of the landform mapping. (c) Detail of the mapping results underlain with image data. Each square has a size of 20×20 km. Legend is on the upper right.

In order to compare our grid-mapping results with independent data and results, we used formal geological maps published by the U.S. Geologic Survey (Greeley & Guest, 1987; Scott & Tanaka, 1986; Tanaka et al., 2005, 2014; Tanaka & Scott, 1987; Figure 13n) and geological and geomorphological maps published in other studies (e.g., Ivanov et al., 2014, 2015). We discuss our findings in section 4.

2.3. Mapping Approach

The mapping of small-scale landforms over vast areas is a challenging task, because it requires both a homogeneous data set and a small mapping scale. Traditional geomorphological mapping (Bishop et al., 2012; Smith et al., 2011; Wilhelms, 1990) is not feasible in this case as it is too time consuming. To enable identification of the presence and distribution of landforms that are relevant to the questions addressed in this study, we adopted a grid *tick box* approach to effectively determine where the specific landforms are. Here we only describe the basics of the method, a full description of this approach is available in Ramsdale et al. (2017) and Voelker et al. (2017).

Mapping as a team helps to share the work and increases the efficacy to deliver timely results but entails some challenges such as the homogeneity of the outcome. We therefore tried to eliminate subjectivity as far as possible by implementing a multitiered approach: First, the individual landforms (e.g., gullies, scalloped terrain) to be mapped were selected by the respective experts in the team. We then prepared a catalog with several examples of each landform for each team member. Then, we prepared one attribute table for Geographic Information System (GIS) containing all landforms and started to map grids one by one. This enabled us in controlling grids more than one time, double-checking the results so each grid was inspected by at least two mappers. The mappers and their contribution in this study can be seen in Figure 13o.

The mapping area (Figure 1) is divided into a grid system of 20×20 km cells, resulting in a grid of $15 \times 3,119$ cells in east-west and north-south direction, respectively (Figure 13). Each grid cell was inspected visually at a scale of 1:10,000 in ArcGIS 10.2 software environment. The presence of each individual landforms was recorded in a classification system consisting of five classes: "0: not present", "1: present", "2: dominant" or "P: possible," and it was also documented if a grid cell was not covered by data or by low-quality images, "N: no data" (Figure 3). For landforms in a grid cell to be present, it is sufficient that a landform is observed at least once, for example, one single gully in an entire cell would result in a value of 1 for this cell. A landform that is covering an entire cell or abundant in a cell would be classified as dominant (i.e., 2). If there is some uncertainty in the identification of a landform, for example, due to limited image quality or resolution, but the mapper felt that there was sufficient evidence to suggest that this landform was present, it would be classified as "P." We opted to use a Cassini projection (similar to a cylindrical projection rotated by 90°) centered on the 22.5° west meridian to minimize distortion across the full length of the strip.

The results together with additional comments were stored in an attribute table that was used for statistical tests to determine the correlation of landforms to each other and to independent data sets such as geological maps, topography, or derived data products (e.g., slopes, roughness). To visualize the results for a given landform, each cell of the grid was colored according to its class (Figure 3), enabling a quick assessment of its spatial distribution across the whole strip. When overlain on context maps, this forms a digital geomorphological map.

2.4. Landform Selection

The first step of this approach is the definition of landforms to be mapped, based on the literature and a reconnaissance survey in GIS. We focus on landforms that are associated with past and present ice- and water-related processes or are relevant to assess the context of landscape evolution. We mapped 13

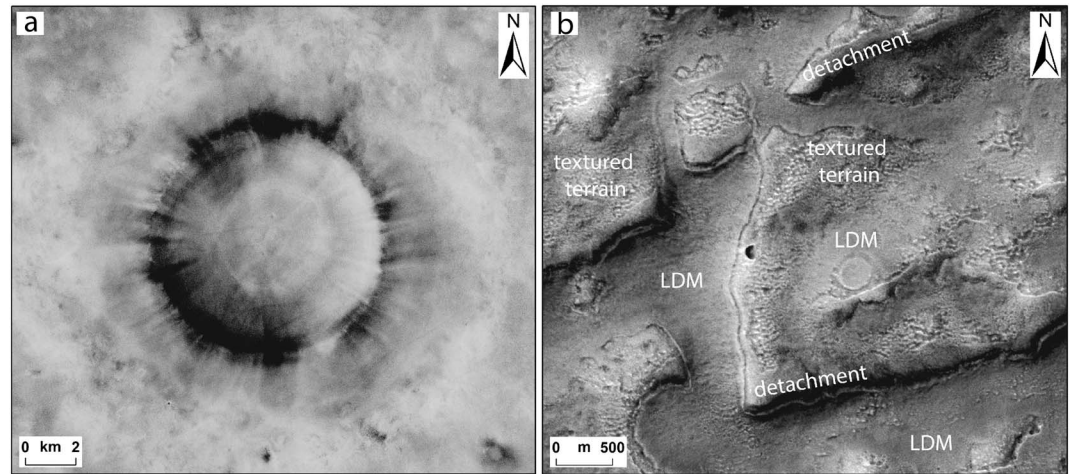


Figure 4. Latitude dependent mantle (LDM) versus textured terrain. (a) Smoothened, subdued topography by LDM from 40–44°N to 78°N. (P17_007612_2447_XN_64N024W). (b) Patches of textured terrain on Acidalia Colles region between 36–43°N and 79°N. Detachment of mantle material and/or viscous flow features is common at the inflection point of the slope (B19_016895_2251_XN_45N024W).

geomorphological features that are listed in Table 1, and representative examples are shown in Figures 4–12. Additionally, we prepared supporting information S1 with examples of grids with landform being *present*, *dominant*, and *possible*, respectively. Moreover, we added additional examples of each landform. We describe each landform here and our findings in section 3.1.

The LDM occurs at the middle and high latitudes of Mars and is composed of a layered mixture of fine-grained ice and dust deposits (Kreslavsky & Head, 2002a; Mustard et al., 2001; Soderblom et al., 1973). The typical LDM is characterized by a smooth surface, which clearly overlies and mantles older terrains and is thus the stratigraphically youngest geological unit on the surface. The thickness of these layers varies from 1 to 10 m (Mustard et al., 2001), but Conway and Balme (2014) estimated a thickness of the LDM from gully incisions that range between 3 and 94 m (average 27 m). This smooth and geologically young (Late-Amazonian Epoch) deposit represents the result of recent climate changes on Mars (Figure 4a). The uppermost mantling layer could have been formed during the last high-obliquity peak 0.4–2 Myr ago (Head et al., 2003). The exposure of recent subsurface ice on steep, pole-facing scarps at the midlatitudes indicates a significant mass of pure ice (<100 m) in mantle deposits that is not in equilibrium with the atmosphere (Dundas et al., 2018).

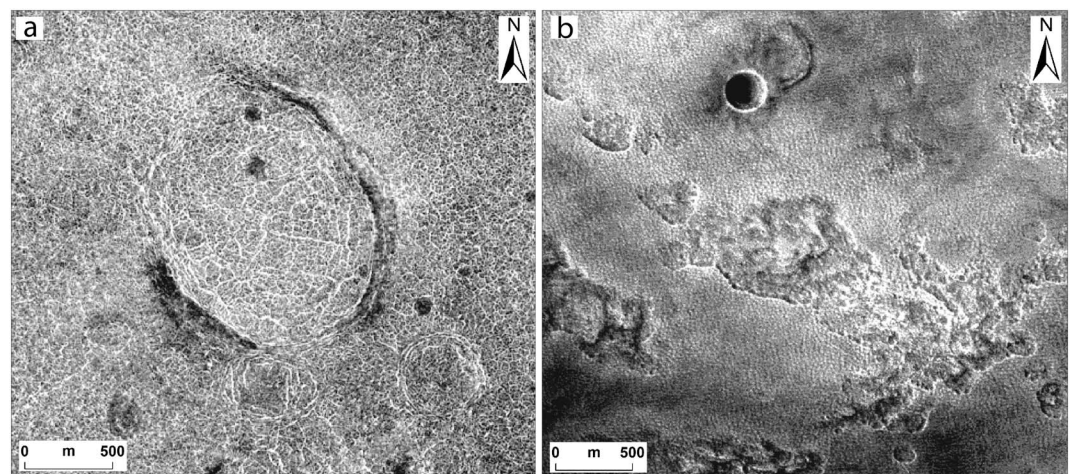


Figure 5. Degradation features related to the latitude dependent mantle. (a) Small-scale polygons on intercrater plains and on crater floors from 51°N to 74°N. (P17_007770_2478_XN_67N019W). (b) Scalloped terrain is confined to the Acidalia Colles region between 46°N and 57°N and positively correlated with the distribution of viscous flow features and latitude dependent mantle (P19_008535_2289_XN_48N024W). The surrounding area shows textured terrain.

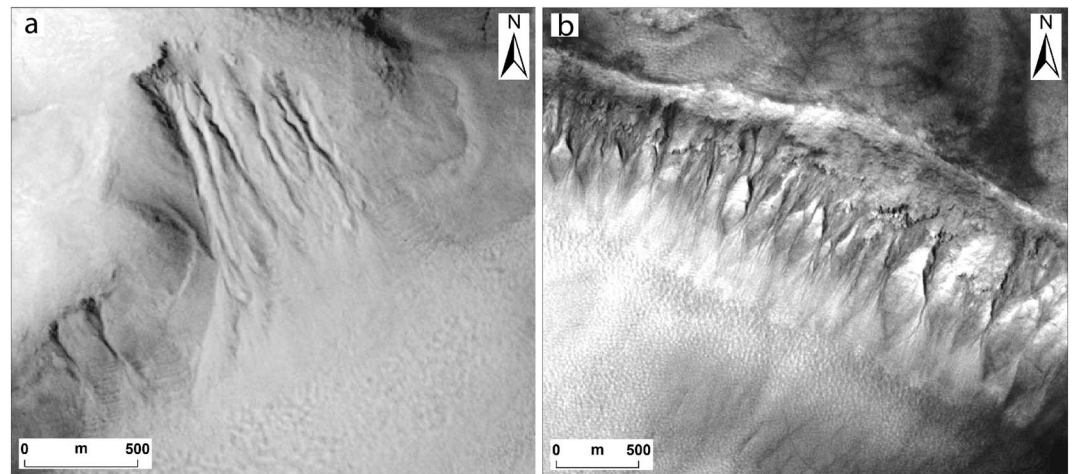


Figure 6. Gullies are located between 32°N and 53°N. (a) Gullies on Acidalia Colles region with pronounced head, channel, and apron structures incised in latitude dependent mantle (LDM). (D02_028156_2256_XI_45N022W). (b) Gullies on crater wall with similar details like in subset “a”. the crater floor is characterized by “intact” LDM and textured terrain, which indicate the dissection of LDM (B16_015906_2317_XN_51N025W).

Textured Terrain is characterized by a type of small-scale surface pattern that was described as “wrinkled,” “pitted,” “brain,” or “basketball” terrains by previous studies (Kostama et al., 2006; Levy et al., 2009b; Mangold, 2005; Mellon et al., 2008). The basketball-textured surface forms evenly spaced, dome-shaped knobs that appear to be arranged randomly or in linear structures, whereas the wrinkle-textured surface type is composed of linear structures on gently sloping hills. The brain terrain displays undulating topography, which forms curvilinear ridges with a spacing that is commonly ~20-m wide (Kostama et al., 2006). We refer to these modification or dissection features of LDM as “textured terrain,” because we were not able to resolve further details at CTX-scale. These degradation processes on the surface of ice-rich landforms indicate the dissection of LDM. There have been recent changes in insolation and climate (Head et al., 2003) at the latitudes where such degradational features are mostly observed (>50–55°N; Mangold, 2005; Kostama et al., 2006).

Small-Scale Polygons are orthogonal and hexagonal networks of polygons with diameters of tens to hundreds of meters, located on intercrater plains and on crater floors. Their plan view shape is morphologically consistent with that of thermal contraction cracks. Various types of thermal contraction cracks have been proposed, such as ice wedge polygons (Soare, Conway, & Dohm, 2014), sand wedge polygons (Séjourné et al., 2011; Soare et al., 2011; Ulrich et al., 2010), or sublimation-type polygons (Levy et al., 2009a, 2010; Marchant & Head III, 2007). However, an origin as desiccation cracks also appears possible, especially for polygons on some crater floors (El Maarry et al., 2010).

Scalloped Terrain consists of isolated or coalesced shallow, rimless, asymmetric depressions of varying sizes, exhibiting steeper poleward facing scarps. Their origin is probably related to thermokarst and the substantial loss of excess ice (i.e., ice exceeding the natural pore water content in a nonfrozen state). Scalloped terrain was proposed to be the result of the ground-ice melting and subsequent evaporation of meltwater (Costard & Kargel, 1995; Soare et al., 2008, 2011). Alternatively, those features may have been formed by the sublimation of ground ice and removal of the remaining sublimation lag by aeolian processes (Lefort et al., 2009, 2010; Morgenstern et al., 2007; Séjourné et al., 2011; Ulrich et al., 2010; Zanetti et al., 2010).

Gullies are systems of erosional and depositional landforms characterized by a head alcove, incised channel, and debris apron (Malin & Edgett, 2000) with lengths of up to a few kilometers and possibly indicative of liquid water, supplied by the melting of snow packs (Christensen, 2003) or near-surface ground ice (Costard et al., 2002). Alternatively, their formation may be a result of *dry* flow processes (Pelletier et al., 2008; Treiman, 2003) involving CO₂ ice (Dundas, Byrne, & McEwen, 2015; Dundas, et al., 2017). They can overlap each other, indicating a formation by episodically occurring, subsequent processes.

Pits have circular, elongated, or irregular plan view shapes and reach diameters of up to a few hundred meters. They may have raised rims. We do not map pits that are degradational landforms in typical LDM,

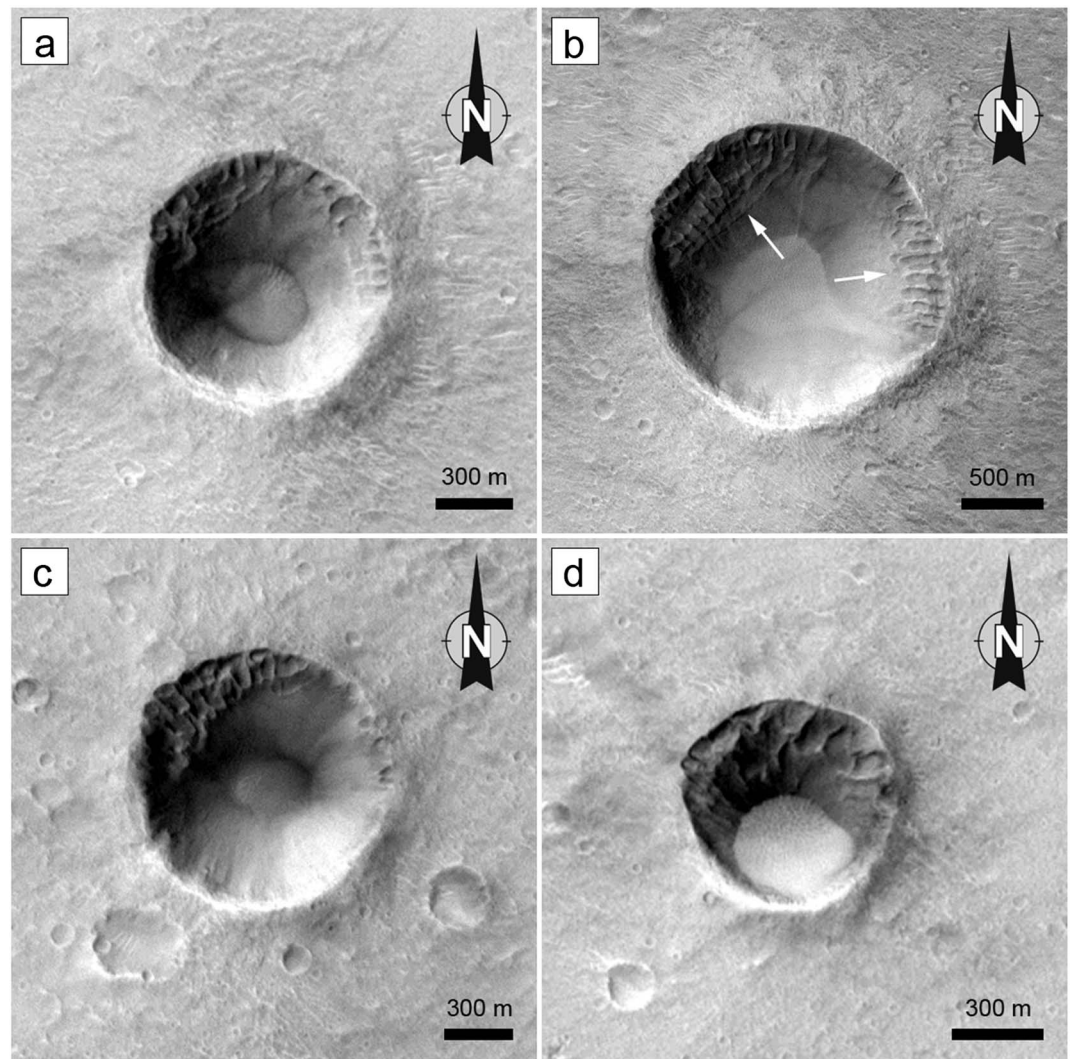


Figure 7. Pits with raised rims on equator-facing crater walls. The pits occur on the highest (i.e., steepest) parts of the inner crater walls and do not resemble mass wasting features such as gullies. Note the location on slopes with different aspect in panel b (white arrows), which is inconsistent with a control by unidirectional winds. (a) Detail of CTX image B20_017396_2085 at 29.03°N/339.045°E. (b) B20_017396_2085 at 28.91°N/339.32°E. (c) B21_017818_2082 at 28.89°N/337.84°E. (d) B21_017818_2082 at 28.34°N/338.18°E.

but rather those that are associated with bedrock material and exhibit the further described morphology in sections 3.1.6 and 4.3.

Large-scale *VFF* are identified along the dichotomy boundary between the northern lowlands and southern highlands by previous studies: Lobate Debris Aprons (LDA), Lineated Valley Fills (LVFs), and Concentric Crater Fills (CCFs) (e.g., Fassett et al., 2014; Head III, Marchant, et al., 2006; Head III, Nahm, et al., 2006; Levy et al., 2009b, 2014; Milliken et al., 2003; Squyres, 1978, 1979; van Gasselt et al., 2010). The term “large-scale *VFF*” has been used by Milliken et al. (2003) to define large-scale ice-related features (LDA, LVF, and CCF); therefore, we refer to these throughout the text. Head III, Marchant, et al. (2006) and Head III, Nahm, et al. (2006) suggested that the LDAs represent debris-covered glaciers with relatively pure ice (Holt et al., 2008; Plaut et al., 2009) derived from snowfall during a glacial period and show an extended lobe at their distal point similarly to piedmont-type glaciers on Earth (Lucchitta, 1981). LVFs are remnants of valley glacial land systems commonly represented by multiple branches of valleys. CCFs appear on crater floors, where the ice-rich material moved downslope from the crater wall (Weitz et al., 2018). In Acidalia Planitia the most common features are LDAs and CCFs.

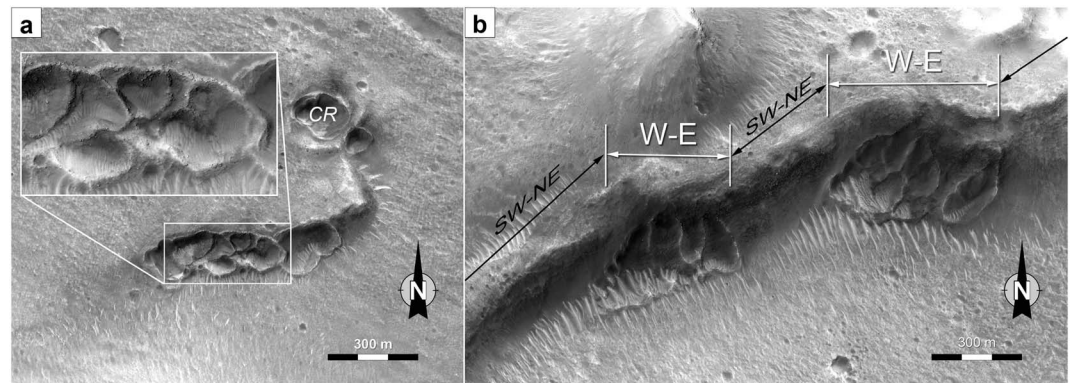


Figure 8. Pits with irregular plan view shapes and raised rims on equator-facing scarps between 24°N and 36°N. (a) Pits with irregular plan view shapes and raised rims containing numerous boulder-sized blocks (see inset). A pit with a continuous concentric raised rim is marked “CR” (for details see text). (b) Pits occur only where the orientation of the scarp is east-west (marked by white arrows) and do not occur where it is SW-NE (black arrows), suggesting that insolation may control pit formation. Note eolian bedforms in pits. Both images are details of High Resolution Imaging Science Experiment image ESP_026521_2130, centered at 32.942°N/336.766°E.

Kilometer-Scale Polygons or giant polygons are outlined by delineating troughs with an average depth of ~30 m and spacing of 5 to 10 km. Their origin might be related to sediment expulsion (Allen et al., 2013; Berndt et al., 2012; Buczkowski et al., 2012; Moscardelli et al., 2012; Oehler & Allen, 2010; Orgel et al., 2015) or elastic rebound after unloading of water or ice from the ground (Hiesinger & Head, 2000).

Large Pitted Mounds (LPM) are positive topographic features with a domical or pie-like cross-sectional shape and typically exhibit a summital pit (Oehler & Allen, 2010). They have circular to subcircular plan view shapes and basal diameters of hundreds of meters to over a kilometer (150 measured: 300–2,200 m, average: 830 m, Oehler & Allen, 2010). LPM are characterized by a high albedo relative to the surrounding plains. They were interpreted to be related to rapid sedimentation of fluid-rich sediment, dewatering and fluid expulsion processes (similar to terrestrial mud volcanism (Allen et al., 2013; Farrand et al., 2005; McGowan, 2009; Oehler & Allen, 2010; Orgel et al., 2015; Salvatore & Christensen, 2014; Skinner, 2012) or impact-related, seismically induced liquefaction (Skinner et al., 2008).

Here we mapped LPM as high albedo, circular, domical features with summital pit using THEMIS and CTX data together. On THEMIS data, LPM can be distinguished from thumbprint terrain (TPT), because LPM exhibit “dark”, circular features, but TPT does not. LPM can appear as coalesced mounds in line, similar to TPT (described below), but when each mound exhibited the above described characteristics, we still mapped them as LPM, rather than TPT.

Small Pitted Mounds (SPM) are high albedo features and have the same morphology to LPM, but smaller in size with an average basal diameter of 170 m (this study). They generally occur in clusters, but are also found solitarily (Farrand et al., 2005; Orgel et al., 2015).

TPT consists of uniformly sized cones that are characterized by multiple-summit pits and have an average basal diameter of 455 m (Farrand et al., 2005). TPT is typically arranged in curvilinear chains of mounds or forms contiguous ridges. Multiple origins have been proposed for the TPT: cinder cones (Plescia, 1980), sublimation (Grizzaffi & Schultz, 1989) or lacustrine features (Lockwood et al., 1992), mud volcanoes (Davis & Tanaka, 1995; Farrand et al., 2005; Orgel et al., 2015), tuff cones (Bridges et al., 2003), phreatomagmatic features (Bruno et al., 2004), and devolatilized pyroclastic flows (Ghent et al., 2012). Individual cones of TPT have smaller sizes than LPM.

Massive ice refers to exposed surface ice (e.g., inside polar craters; Conway et al., 2012) as well as the polar cap itself.

Bedrock is defined here as outcrops of rock, commonly on slopes. It can be exposed by the detachment of ice-bearing material or by a crater-forming impact. Here we refer to all materials as bedrock that are not covered by LDM (Figures 7–9 and 12).

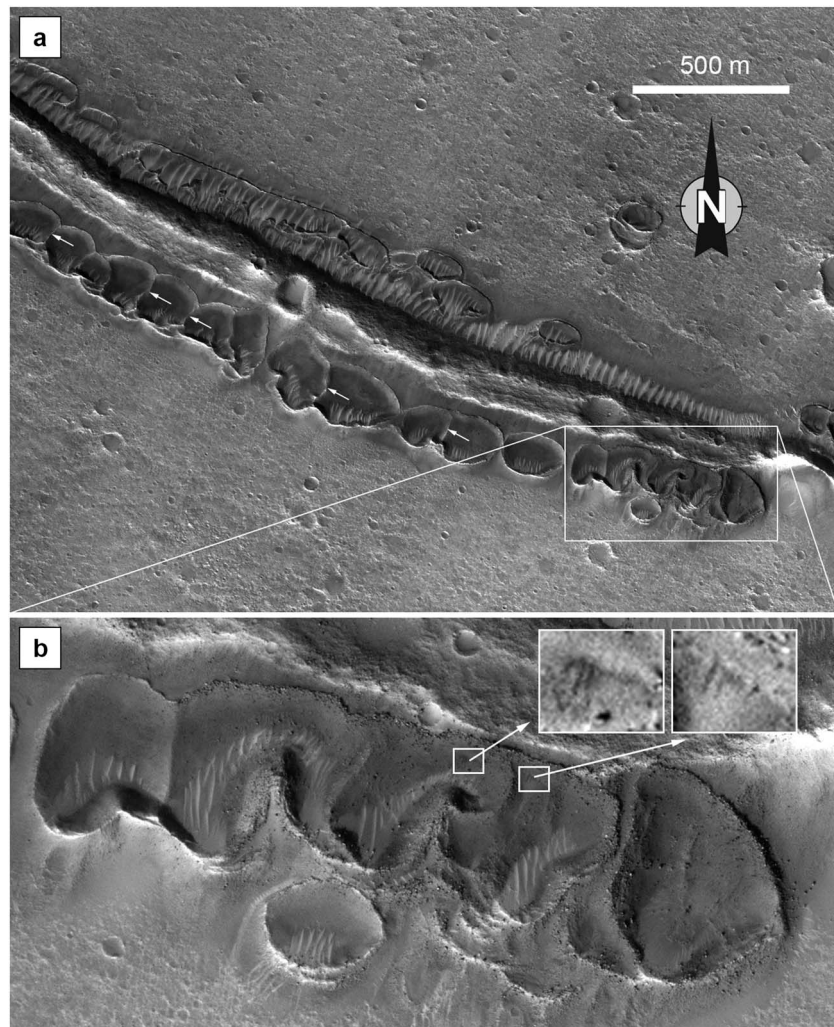


Figure 9. Pit chains along topographic ridge. (a) Pits with circular to irregular plan view shapes are larger and more densely spaced on equator-facing (sunlit) slope than on pole-facing slope. The thin ridges separating individual pits are more or less rectilinear (white arrows), suggesting that the pits formed simultaneously. (b) Enlarged part of Figure 9a. boulders are numerous and appear to be concentrated at rims. The two insets show dark slope streaks or potential recurrent slope lineae. Detail of HiRISE image ESP_026521_2130 at 30.959°N/339.402°E.

3. Observations

3.1. Grid-Mapping Results

In this section, we present the grid-mapping results (Figure 13), especially focusing on the latitude, elevation, and slope dependence of the landforms visualized by the box plots (Figure 14 and supporting information S2).

3.1.1. LDM

Based on our grid mapping, local LDM deposits first appear poleward already at latitudes slightly north of 40°N, where it is still gradational with the bedrock. LDM is unambiguously present further north from 44°N to 78°N and dominates the Acidalia Colles region and north of that (Figure 13a).

3.1.2. Textured Terrain

LDM (Figure 4a) and textured terrain (Figure 4b) almost completely overlap in the whole mapping area; hence, they strongly and positively correlate with each other. The textured terrain has ambiguous occurrences at 36°N, is present between 43°N and 79°N, and dominates between 45°N and 77°N, similarly to the occurrences of LDM (Figure 13b). LDM and textured terrain cover a relatively broad elevation range, including partly the Acidalia Colles from $\sim -4,700$ to $\sim -5,600$ m, but 50% of the landform occurs at around $-5,000$ m.

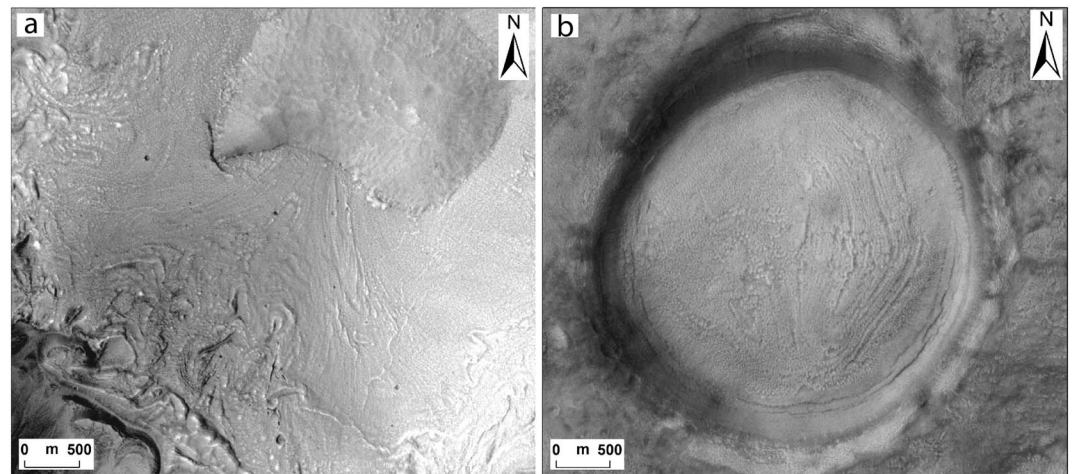


Figure 10. Large-scale viscous flow features (VFF) between 36°N and 53°N. (a) VFF inside a crater. (b) Crater with CCF, covered by LDM and textured terrain (B17_016407_2186_XI_38N021W).

The textured terrain is further present at slightly higher elevations of $\sim -4,600$ m and commonly located in the same latitude range as LDM. Similarly, LDM and textured terrain are present on slopes of up to 3.3° , but commonly on gentle slopes between 0.6° and 1.3° . In the Acidalia Colles region, they appear on steeper slopes up to 10° (Figure 14). The distribution of textured terrain is consistent with previous studies (Kostama et al., 2006; Mangold, 2005), but our observations indicate textured terrain at latitudes north of those reported by Kostama et al. (2006).

3.1.3. Small-Scale Polygons

Small-scale polygons occur most commonly from 51°N to 74°N but are heavily concentrated between 61°N and 72°N (Figures 5a and 13c) on the intercrater plains and on the floors of filled impact craters. They occur within a narrow elevation band from $-5,037$ m to $-5,154$ m and 50% of the features are dominant at $\sim -5,100$ m, which is a slightly lower elevation than the main concentration of LDM and textured terrain. They appear on almost flat surfaces of $<1^\circ$ slopes, but extreme cases show slopes up to 1.5° (Figure 14). The spatial distribution of these polygons is very similar to that of the LDM and textured terrain, supporting the hypothesis of a dissected LDM. The distribution of small-scale polygons in our mapping is in good agreement with previous studies (El Maarry et al., 2010; Kostama et al., 2006; Levy et al., 2009a; Mangold, 2005; Mellon et al., 2008).

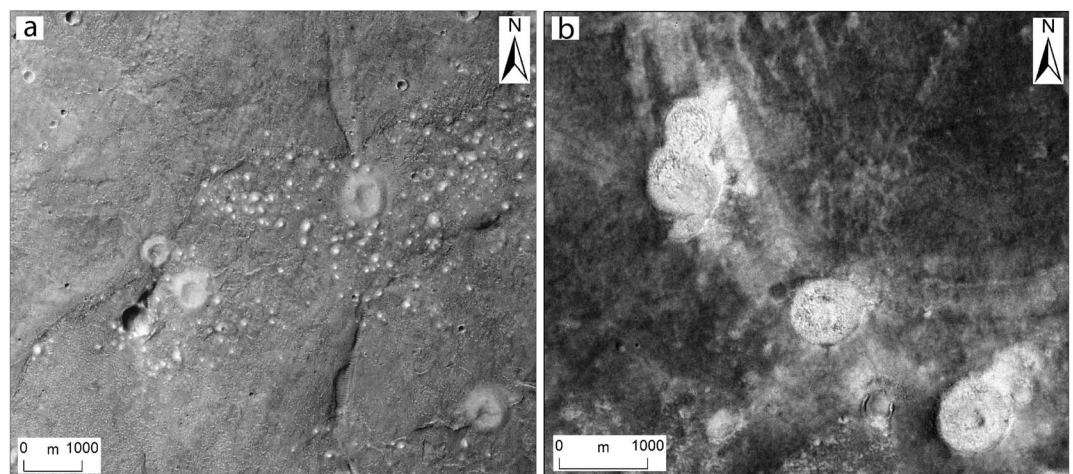


Figure 11. Possible water-related sedimentary structures predating the LDM. (a) Kilometer-scale polygon troughs (from 35°N to 48°N and from 54°N to 63°N) occur with high-albedo dome-type large pitted mounds (38°N – 54°N) and clustered small pitted mounds (34°N and 48°N ; B19_017185_2220_XN_42N021W). (b) Pie-type large pitted mounds (48°N – 54°N ; F03_036806_2280_XN_48N019W).

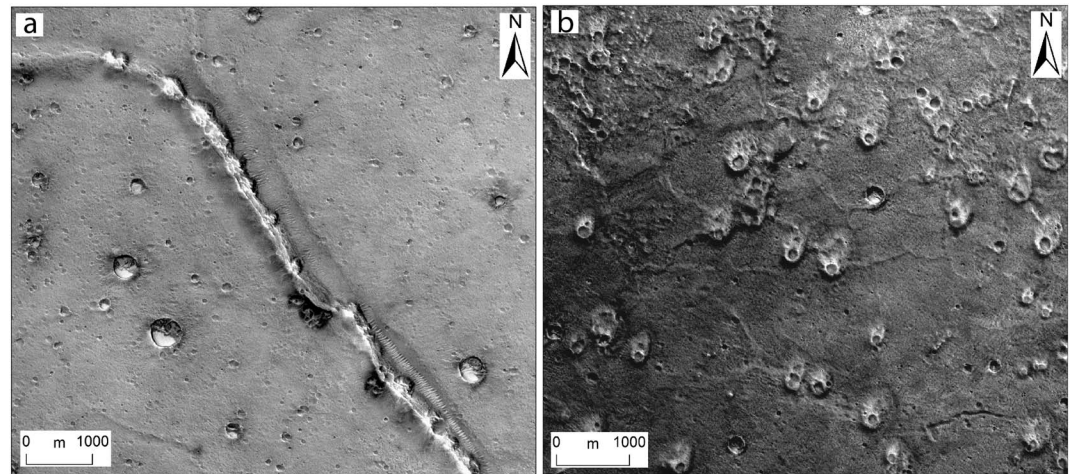


Figure 12. Possible water-related aggradational structures predating latitude dependent mantle. Thumbprint terrain is located between 30°N and 39°N in the southern Acidalia Planitia. Morphology of thumbprint terrain varies from the south to the north. (a) Curvilinear, ridge-like feature with hardly recognizable cones around 30°N (B16_016051_2121_XN_32N020W). (b) Single thumbprint terrain cones (D16_033536_2134_XN_33N023W) partly connected with ridge-like features around 33°N, but ridges are less prominent as in image Figure 12a.

3.1.4. Scalloped Terrain

In Acidalia Planitia, scalloped terrain can only be found within a limited latitude range between 46°N and 57°N and is mostly concentrated in the Acidalia Colles region (48–53°N; Figures 5b and 13d). All observed isolated scalloped depressions in Acidalia Planitia are characterized by a diameter of <100 m and are less prominent features than in Utopia Planitia (Morgenstern et al., 2007; Séjourné et al., 2011; Séjourné et al., 2018). Scalloped terrain cooccurs with the LDM and textured terrain but is surprisingly less correlated with the small-scale polygons. The scalloped terrain occurs at elevations from $\sim -4,600$ m to $\sim -5,000$ m, but 50% of the landforms are concentrated between $\sim -4,700$ m and $\sim -4,900$ m, similarly to VFF. The slope distribution of scalloped terrain ranges from 1.4° to 7°, but half of the population occurs on slopes between 2.8° and 5.7° (Figure 14).

3.1.5. Gullies

Gullies are observed within a limited latitude range between 32°N and 53°N (Figure 13e) in Acidalia Planitia. The clustered gully distribution in the Acidalia Colles region (Figure 6) is also the area with the highest gully density in the northern hemisphere (Harrison et al., 2015), likely due to the occurrence of relatively steep hill-slopes in this area (Figure 2), which is a prerequisite for gully formation (e.g., Reiss et al., 2009). Gullies appear at elevations from $\sim -4,300$ m to $\sim -4,900$ m, but the half of the population occurs between $\sim -4,500$ m and $\sim -4,800$ m with a median of 4,686 m (Figure 14). The orientation of gullies in the Acidalia Mensa and Acidalia Colles region between 44°N and 53°N latitude shows a strong equatorward orientation (Canzler, 2014; Decker, 2015), whereas gullies located at latitudes <44°N predominantly occur on poleward facing slopes (Figure 13e), which is consistent with mantle-free bedrock. This gully distribution within a limited latitude range is in agreement with previous gully studies in the northern hemisphere (Bridges & Lackner, 2006; Harrison et al., 2015; Heldmann et al., 2007; Kneissl et al., 2010) and consistent with an orientation preference observed in the southern hemisphere on Mars (Balme et al., 2006; Dickson et al., 2007).

3.1.6. Pits

Pits occur mostly in the southern part of Acidalia Planitia, to the west and northwest of Cydonia Mensae. They are preferentially located on equator-facing slopes, for example, on the inner walls of impact craters (Figure 7) or on the flanks of wrinkle ridges, thumbprint terrain, or other landforms with positive topography (Figures 8 and 9a). They are found on regional slopes up to 3.2°, but commonly on gentler slopes between 0.7° and 1.8° (Figure 14). They occur as isolated features but most commonly form clusters (Figure 7) or chains (Figure 9). Many individual pits in a pit chain seem to have formed more or less simultaneously, based on the observation that ridges separating the pits do not indicate a superposition of one pit on top of another one (Figure 9a). On the other hand, smaller pits may occasionally be nested in larger ones, suggesting that separate episodes of pit formation may have occurred. The pits appear to be relatively shallow and have raised

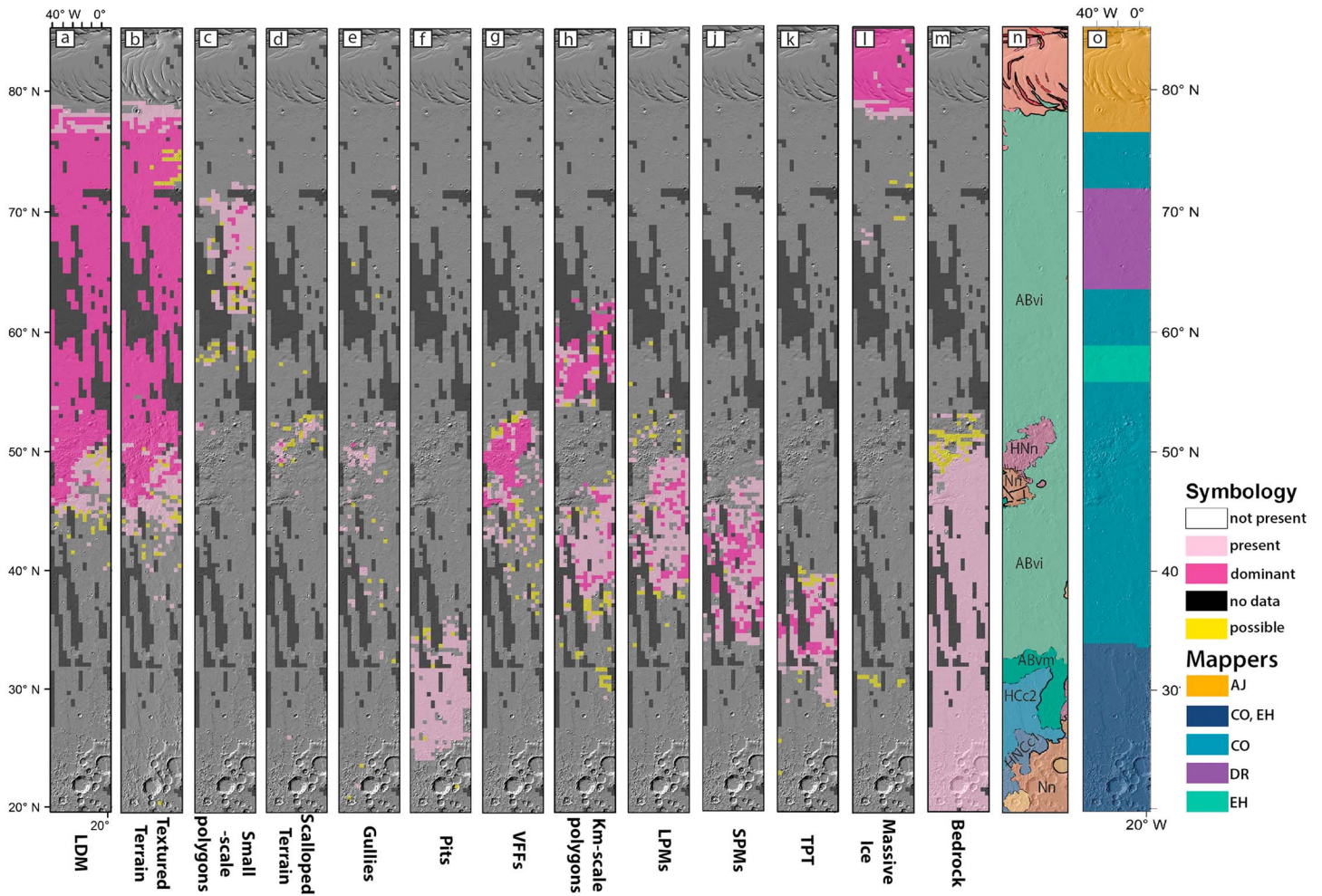


Figure 13. Grid-mapping results of landform distribution with MOLA hillshade background from latitude 20° to 84°N. 0 = No occurrence; 1 = landform present; 2 = landform dominant, P = possible occurrence, N = no data. (a) Latitude-dependent mantle (LDM); (b) textured terrain; (c) small-scale polygons; (d) scalloped terrain; (e) gullies; (f) pits; (g) viscous flow features (VFF); (h) kilometer-scale polygons; (i) large pitted mounds (LPM); (j) small pitted mounds (SPM); (k) thumbprint terrain (TPT); (l) massive ice; (m) bedrock; (n) geology: Noachis Terra unit (Nn), crater (AHc) and crater floor (AHcf) units, Chryse Planitia 1 (HNCc1) and 2 (HNCc2) units, Nepenthes Mensae (HNn), Vastitas borealis formation interior (ABvi) and marginal (ABvm) units (Tanaka et al., 2014); (o) mappers: CO = Csilla Orgel, EH = Ernst Hauber, AJ = Andreas Johnsson, DR = Dennis Reiss.

rims, which partly consist of boulder-sized blocks (Figures 8a and 9b). The floors of some pits are partly covered by aeolian bedforms (Figures 8b and 9b). No evidence of fluvial activity or runoff, for example, erosional channels, can be observed in association with the pits. However, some small low-albedo features may be dark slope streaks or potential recurrent slope lineae (RSL; Figure 9b).

Pits are concentrated between 24°N and 36°N (Figure 13f) and their occurrence does not overlap with LDM, but it does coincide with the lower boundary of the textured terrain around 36°N, which suggests a possible relation to past extent of LDM and thus volatiles. Pits are located from ~−3,800 m to ~−4,100 m, frequently between ~−3,900 and ~−4,000 m and overlap with the elevation outliers of textured terrain (Figure 14).

3.1.7. Large-Scale VFF

VFF in Acidalia Planitia are located between 36°N and 53°N (Figure 13g) and concentrated on the hilly area around the Acidalia Colles (Figures 4b and 10) and north from that. South from the Acidalia Colles region, VFF occur predominantly in craters. About 82% of VFF are concentrated within this region between elevations of −4,528 m and −4,927 m and 50% of VFF are confined between −4,633 m and −4,842 m (Figure 14). VFF are present on slopes between 1° and 6°, which is not surprising, as by definition their formation requires elevation differences (Figure 14). The Acidalia Colles hills are not only covered by VFF, but LDM and textured terrain occur here as well. The detachment of ice-rich material from the hills results in the

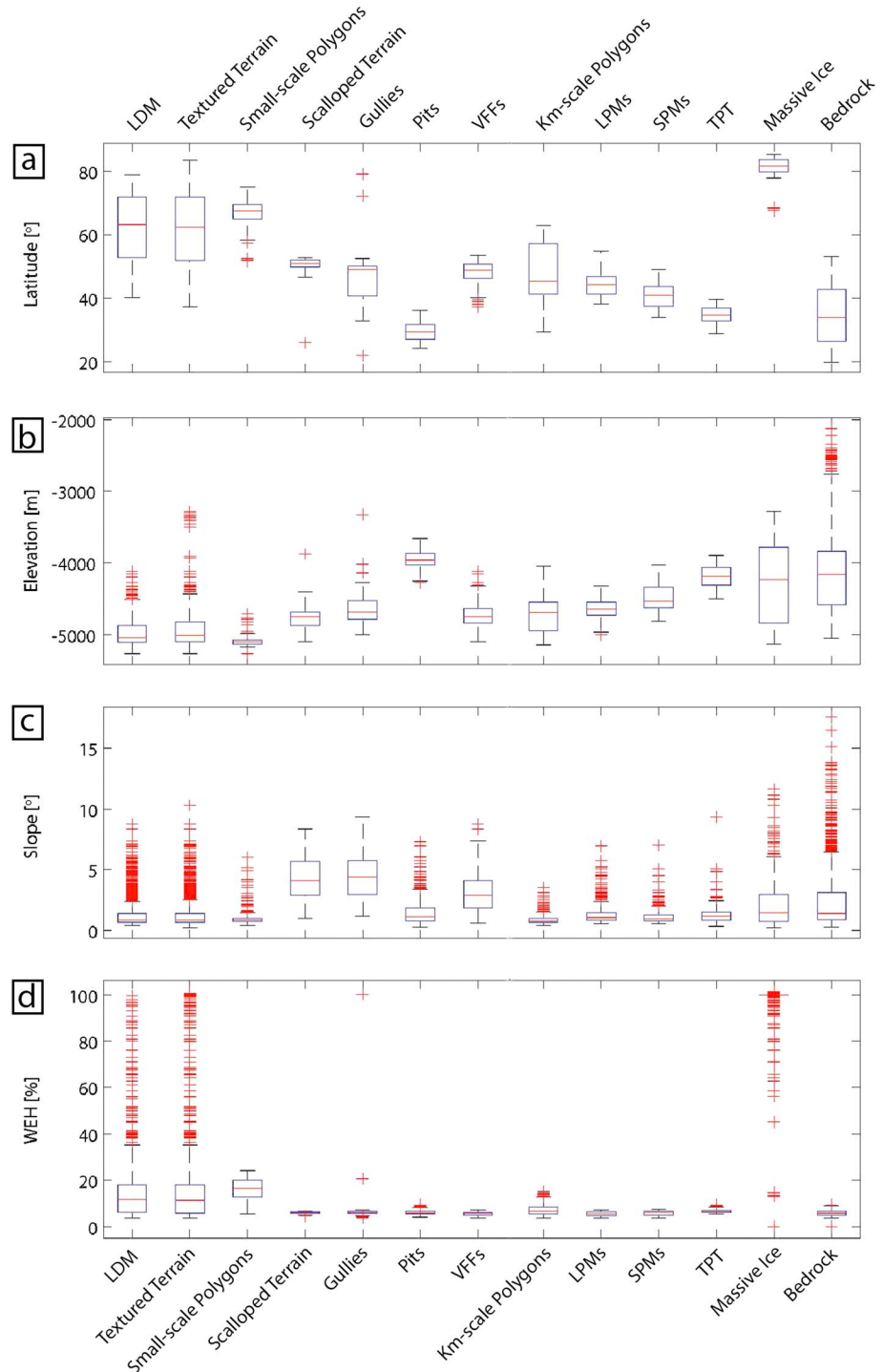


Figure 14. Range of occurrence of landforms in relation to their (a) mean latitude, (b) elevation, (c) slope, and (d) WEH in Acidalia Planitia (Wilson et al., 2018). Five values are used to display the distribution: The first three are in the interquartile range (IQR) or box, which is composed of the upper (Q3) and lower (Q1) quartiles, and the median (Q2; red line). The box defines the cells where the landform occurs in the 25–75% IQR in a normal distribution, meaning that it contains 50% of the population. The fourth element is the whisker below (Q1–1.5*IQR) and above (Q3 + 1.5*IQR) the box, this represents the 9–91% quartiles, including 82% of the populations. The fifth value shows the outliers which fall below or above the whiskers and are distant points from observations observation (red cross; Frigge et al., 1989; McGill et al., 1978). We show the specific values in the supporting information S2.

exposure of bedrock or the occurrence of very thin mantling deposit in these places, suggesting ice deformation and ice mass movement processes (Figure 4b). It seems likely that VFFs are covered by LDM, or thick LDM forms the VFF in this region, which we will discuss in detail in section 4.

3.1.8. Kilometer-Scale Polygons

Localized occurrences of giant polygons are present from 30°N poleward, but most form two separate populations from 35°N to 48°N and from 54°N to 63°N, respectively, and dominate between 38°N–39°N and 54°N–62°N (Figure 13h). The southern population is partly subdued by LDM and textured terrain, whereas the northern population is completely covered by LDM. Their spatial distribution overlaps with that of the LPM, SPM, and partly with that of the TPT (Figure 12). These giant polygons do not overlap with the small-scale polygons, which are situated further north in the study area. However, the kilometer-scale polygons may be partly hidden from observation beneath the youngest mantle if that is thick enough, masking the true total distribution of the large polygons. The kilometer-scaled polygons completely disappear at the Acidalia Colles region and northward, thus it seems that the low-lying, flat areas are more favorable for their emplacement. They appear between $\sim -4,500$ m and $\sim -5,000$ m elevation on slopes from 0.5° to 1.3° with a median of 0.8° (Figure 14). The distribution of giant polygons in our mapping area is consistent with results presented by Oehler and Allen (2010).

3.1.9. LPM

LPM in the Acidalia mapping area are located further north than TPT and occur isolated or arranged in clusters between 38°N and 54°N and disappear completely at 59°N and further poleward (Figure 13i). LPM are spatially associated with the kilometer-scale polygons and SPM, as LPM appear within the giant polygons (Figure 11a). The extent of LPM is restricted to the Vastitas Borealis Formation, and LPM do not occur in the topographically elevated region of the Acidalia Colles region. With respect to their elevation, they occur from $\sim -4,800$ m to $\sim -4,500$ m and typically on slopes of less than $<1.5^\circ$ (Figure 14). There is a gradational, morphological transition zone from (south to north) TPT to LPM at around 38°N. Around 39°N and northward, only LPM without TPT can be observed. The morphology of LPM also varies from the southern dome-type mounds to the northern pie-type population at 48°N (Figure 11b). SPM appear with the dome-type LPM, but SPM cannot be observed with the pie-type LPM. The pie-type mounds are associated with the southern extent of the LDM and textured terrain. Noticeably, LPM are overlain by LDM and textured terrain, suggesting that there is a significant mantle coating on the mounds from 44°N poleward. The distribution of LPM in our mapping is in agreement with results obtained by Oehler and Allen (2010) and Skinner (2012).

3.1.10. SPM

SPM are located between 34°N and 48°N and completely overlap with areas where dome-type LPM and partly the TPT occur (Figure 13j). SPM features can occur isolated and randomly distributed or in closely spaced clusters (Figure 11a). They appear to be spatially associated with the larger-sized mounds (LPM and TPT).

3.1.11. TPT

TPT occurs in various morphologies between 30°N and 39°N close to the distal end of the outflow channels and is dominant from 33°N to 39°N (Figure 13k). Topographically, it occurs between $\sim -4,000$ m and $\sim -4,400$ m and mostly on slopes of $<1.5^\circ$ (Figure 14). Curvilinear, ridge-like features with hardly recognizable individual cones are present at around 30°N (Figure 12a). Individual cones appear at 33°N in clusters or solitarily, and ridge-like features connect the single cones (Figure 12b), though further north in the strip those ridges disappear between the mounds. TPT shows a morphological transition zone with the LPM around 38°N. TPT cones have smaller basal diameter than LPM and have more pits on their flanks. This landform coexists with SPM up to 34°N. TPT is not observed north of 39°N. This distribution of TPT in our mapping area is consistent with previous studies (Farrand et al., 2005; McGowan, 2009; Oehler & Allen, 2010).

3.1.12. Massive Ice

Massive ice is commonly related to the extent of the northern polar cap between 77°N and 84°N (Figure 13l).

3.1.13. Bedrock

Bedrock is exposed in every grid cell from 20°N up to 53°N (Figures 13m, 7–9, and 12), and between 48°N and 53°N it appears exposed by the detachment of ice-rich material from the hills and plateaus in Acidalia Colles (Figure 4b). The transition between bedrock and LDM appears to be gradational rather than a distinct boundary.

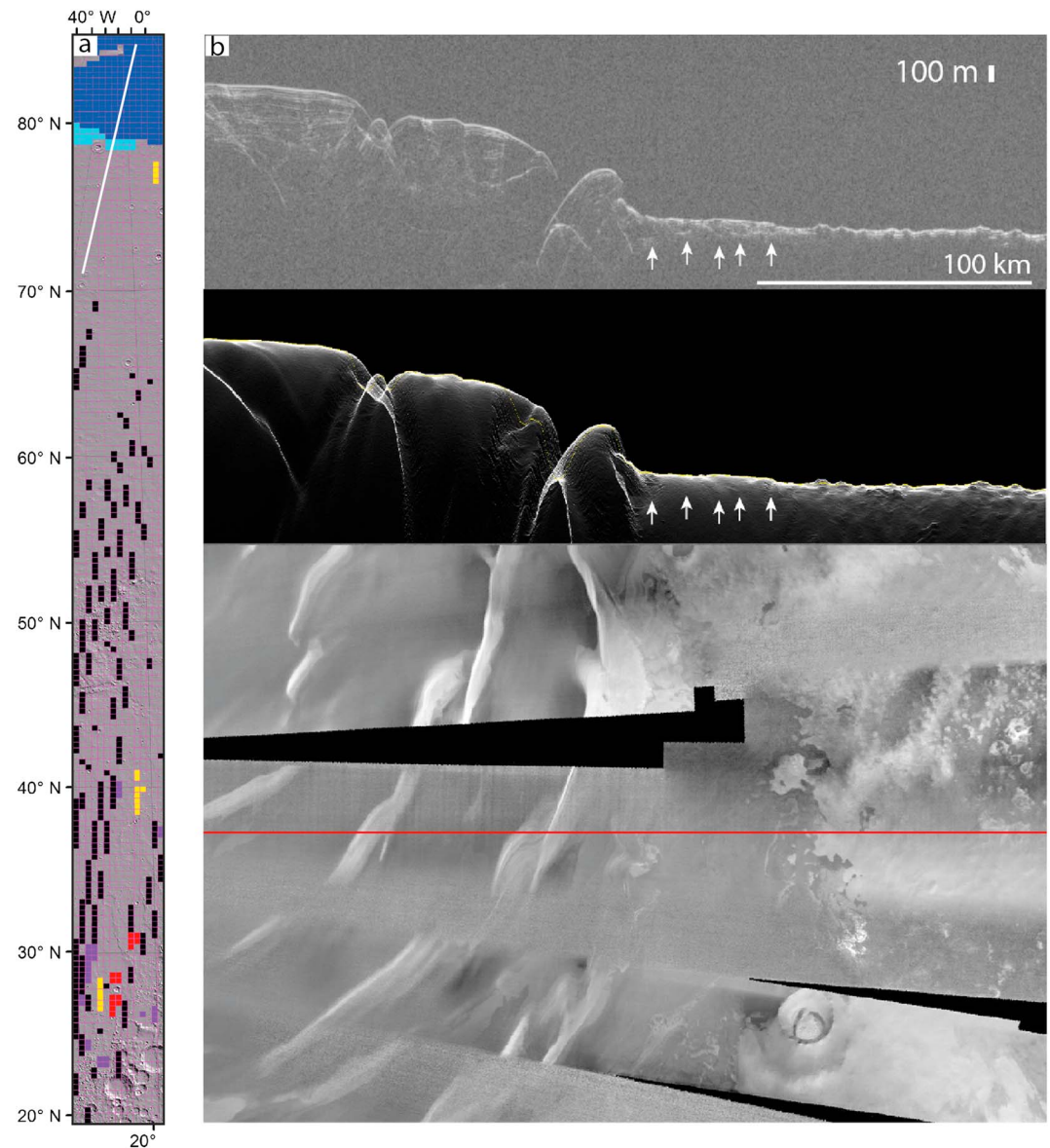


Figure 15. SHARAD observations along the Acidalia Planitia swath. (a) SHARAD subsurface detections with MOLA hillshade background from latitude 20° to 84°N. Dark blue = NPLD; light blue = near the NPLD; red = high confidence detections; purple = low confidence detections; yellow = not correlated to subsurface detection; black = no data. The white line shows the location of the radargram. (b) Subsurface detection of ice near the NPLD (white arrows; 3703–02). The upper image is the radargram, the simulation is in the middle, the bottom image is MOLA DEM. SHARAD = SHARAD; NPLD = North Polar Layered Deposits; MOLA = Mars Orbiter Laser Altimeter; DEM = Digital Elevation Model.

3.2. MOLA Elevation and Roughness

The topography decreases along the swath from $\sim -2,000$ m (south) to $\sim -6,000$ m (north; Figure 2a). Surface roughness at a 9.2-km baseline scale generally decreases from the south to the north and is high in the far south related to the highlands and bedrock material up to 32°N, as well as in the Acidalia Colles region that is characterized by isolated plateaus and hills. A low roughness (smoothing of topography) is characteristic over the majority of the area, north and south from that region (Figure 2b).

3.3. SHARAD

At the northern end of the mapped swath the North Polar Layered Deposits and outlier deposits dominate the subsurface signal (Figure 15b). We mapped those reflectors as dark blue and light blue, respectively

Table 2
Controlling Factors That Potentially Influence the Formation of Landforms

#	Landform/dependency	Latitude	Elevation	Slope	Orientation	Geology
1	Latitude dependent mantle (LDM)	X	—	—	—	—
2	Textured terrain	X	—	—	—	—
3	Small-scale polygon	X	X	X	—	—
4	Scalloped terrain	X	X	X	—	—
5	Gullies	X	X	X	X	—
6	Pits	X	X	X	X	—
7	Viscous flow features (VFF)	X	X	X	—	—
8	Km-scale polygons	—	—	X	—	X
9	Large pitted mounds (LPM)	—	—	X	—	X
10	Small pitted mounds (SPM)	—	—	X	—	X
11	Thumbprint terrain (TPT)	—	—	X	—	X
12	Massive ice	X	—	—	—	—
13	Bedrock	—	—	—	—	—

Note. "X" indicates the dependency of landforms to latitude, elevation, slope, orientation, and/or geology.

(Figure 15a). South of the known surface ice deposits, SHARAD does not detect unambiguously ground surface reflectors in the swath. This is likely because the top and bottom of any subsurface ice is too close to the surface. SHARAD has a vertical resolution of ~15 m.

SHARAD data show subsurface interfaces at lower latitudes in the strip. These likely represent a combination of boundaries between lava flows, ejecta blankets, and sedimentary rocks, where the material is rather rocky than icy. Multiple subsurface signals related to rocks were considered high-confidence detections (red), whereas those with weaker signals were considered low-confidence detections that could be correlated (purple) or not correlated (yellow) with subsurface detections (Figure 15a).

4. Discussion

4.1. Landform Assemblages

Based on the distribution of landforms, we defined four specific landform assemblages (or landform provinces): (1) *Geologically recent* polar cap (massive ice) which superposes the mantle material (LA1); (2) ice-related landforms, such as LDM, textured terrain, small-scale polygons, scalloped terrain, large-scale VFF, and gullies, which have an overlapping distribution (LA2); (3) surface features possibly related to water and subsurface sediment mobilization (LA3; kilometer-scale polygons, LPM, SPM, and TPT); (4) irregularly shaped pits. In the following, we examine in further detail the LA2 (section 4.2) and the pits (4) (section 4.3). LA2 is being discussed as a group, because its features may have a common origin and relation to LDM, which is the focus of this study. The pits are discussed in a dedicated chapter because these features have never been described in detail before. We summarize the controlling factors that influence the formation of landforms in Table 2.

4.2. LDM and Related Landforms

4.2.1. Latitude and Geology Dependence

LDM extends from 40°N–44°N to 78°N and overlaps with the textured terrain almost everywhere in the Acidalia Planitia mapping strip. Its distribution appears independent of geological boundaries as mapped by Tanaka et al. (2014; Figures 13a and 13b). This strongly reconfirms its latitude dependence and the postulated origin as an ice-rich air fall deposit (Head et al., 2003; Kreslavsky & Head, 2002a; Mustard et al., 2001). The dissection of the LDM appears to grade from less severe in the north to more severe in the south. Three other landform types occur within the latitude range of LDM and textured terrain: Small-scale polygons, scalloped terrain, and gullies (Figures 13c–13e). Small-scale polygons are located in the region of dominant LDM and textured terrain. They have been interpreted as thermal contraction cracks in a fine-grained cohesive material (e.g., Levy et al., 2010; Ulrich et al., 2011), and the most straightforward explanation would be that this material is ice-cemented regolith or even excess ice (Levy et al., 2009a, 2010), both in agreement with hypotheses of LDM composition (e.g., Mustard et al., 2001). The small-scale polygons show the same trend of disappearance toward south, which may indicate a LDM that is thinning

toward south, or that is containing less cementing ice, or both. A link to LDM may also be plausible for scalloped terrain and gullies. Scalloped terrain is thought to be a result of thermokarstic degradation of LDM (e.g., Dundas, Byrne, & McEwen, 2015; Lefort et al., 2010; Ulrich et al., 2010), and many gullies are incised into LDM (Dickson et al., 2015). The limited extent of terrain displaying scalloped terrain and gullies within the much larger LDM may be explained by other controlling factors (see sections 4.2.2 and 4.2.3, and Table 2). Bedrock outcrops are exposed in the Acidalia Colles region due to the detachment of mantle or VFF on the slopes of hills and mesas. Bedrock is also present in the southern parts of the mapping area where LDM is absent; hence, its extent is complementary to LDM.

The landform assemblage 3 (LA3) also shows a distribution that seems to be restricted to a certain latitude range (~30°N to 50°N), with an additional region displaying kilometer-scale polygons north of the Acidalia Colles and Mensae (54–63°N). Among the single classes of landforms within the LA3, there is a trend of increasingly northward location of TPT, SPM, LPM, and kilometer-scale polygons. Whereas such a trend could indicate a control by insolation, an alternative interpretation is that a varying thickness of the VBF is responsible. A link between the VBF and both kilometer-scale polygons and LPM has been proposed by previous studies: The VBF has been hypothesized to be the residual deposit of originally volatile-rich effluents from the outflow channels (Kreslavsky & Head, 2002b), and the kilometer-scale polygons are spatially associated with the terminations of the outflow channels (Lucchitta et al., 1986) and have been explained by various processes acting on such sediments (e.g., Allen et al., 2013; Lane & Christensen, 2000; McGill & Hills, 1992). On the other hand, the LPM have been proposed to represent surface manifestations of subsurface sediment mobilization of outflow channel sediments (Hemmi & Miyamoto, 2018; Salvatore & Christensen, 2014). The kilometer-scale polygons cover a relatively large region south and north of the Acidalia Colles and Mensae (Figure 13h), and the LPM occur more or less in the same area as the southern part of the kilometer-scale polygons (Figure 13i). SPM approximately overlap with LPM, but their extent reaches a bit more southward than the latter (Figure 13j). TPT in turn overlaps with the southernmost extent of LPM and with a large part of the region containing SPM (Figure 13k). Taken together, there is a successively more (average) southward extent from kilometer-scale polygons, LPM, SPM, and TPT (Figures 13h–13k), which are all located in, almost flat-lying, very smooth terrain (Figure 2; see also Figure 9 in Campbell et al., 2018). This may suggest that the control on their distribution is some varying property of the VBF, for example, thickness, rather than climate.

4.2.2. Elevation and Slope Dependence

LDM and textured terrain occur over a broad range of elevations (from ~−4,700 m to ~−5,600 m) and slopes (up to 10°); therefore, no evidence exists for elevation or slope-dependency, consistent with a hypothesized origin of LDM as a result of precipitation that drapes all but the steepest underlying relief (Head et al., 2003; Madeleine et al., 2014). In contrast, VFF and gullies are concentrated in the Acidalia Colles region and on impact crater walls, suggesting a strong relation to varying slopes. Of all mapped landforms, gullies occur together with VFF on average on the steepest slopes (Figure 14). As both types of features are thought to be a result of gravity-driven processes (ice creep and debris or granular flows, respectively), this observation is not surprising. Of all mapped landforms, scalloped terrain occurs together with gullies and VFF on average on the steepest slopes (Figure 14). The reason for this is unclear, but local variations in insolation may cause heterogeneities in the stability of subsurface ice, leading to preferential sublimation and thermokarst initiation at steeper slopes (Aharonson & Schorghofer, 2006). Small-scale polygons and scalloped terrain appear commonly in a narrower elevation range than LDM, demonstrating a strong dependency on elevation, although they do not show a common spatial distribution. Small-scale polygons only appear on smooth, flat surfaces with slopes <1°, which would be consistent with an origin as desiccation cracks in ponds as proposed by El Maarry et al. (2010), although it does by no means exclude an origin as thermal contraction cracks. Scalloped terrain occurs on varying slopes between 2.8° and 5.7°, and we observe the concentration of scallops in a narrow elevation range (between ~−4,700 m and ~−4,900 m); thus, the elevation dependence of scalloped terrain is clear. We conclude that this observation, in combination with the latitude dependence of scalloped terrain, suggests an insolation- and climate-controlled origin (see also Dundas, 2017).

4.2.3. Orientation Dependence

We observed a preferential location of gullies on pole-facing slopes at midlatitudes between 32°N and 44°N and on equatorial-facing slopes for more northern gullies, in agreement with previous studies on both the northern hemisphere (Harrison et al., 2015; Heldmann et al., 2007; Kneissl et al., 2010) and the southern

hemisphere (Balme et al., 2006; Dickson et al., 2007). A control of gully formation by insolation (and, at these latitudes, ultimately by obliquity; Schorghofer, 2008) seems therefore the most likely explanation for this latitude-dependent change of orientation dependence. On the other hand, we do not observe a correlation of scalloped terrain and slope orientation (aspect), in agreement with Lefort et al. (2009), who note an apparent absence of orientation dependence. The small, irregularly shaped pits are preferentially located on equator-facing slopes, and we discuss this in section 4.3.

4.2.4. Climatic Implications

Various equilibrium models predict that near-surface ground ice should be stable under current obliquity and orbital conditions poleward of approximately $\pm 50\text{--}55^\circ$ latitude on both hemispheres (Chamberlain & Boynton, 2007; Mellon et al., 2004; Mellon & Jakosky, 1995; Schorghofer & Aharonson, 2005). The distribution of shallowly buried subsurface ice in the uppermost layer of the Martian regolith as measured with neutron and gamma ray spectroscopy (GRS) is consistent with these models (e.g., Boynton et al., 2002; Feldman et al., 2004; Jakosky et al., 2005; Mitrofanov et al., 2004; Wilson et al., 2018). To see the correlation between different data set and model results to our mapping, we refer to our supporting information S3. The extent of dominant LDM as mapped in our study (Figure 13a) is broadly (but not perfectly, see below) consistent with both the GRS results (Figure 14d) and the models of ice stability and supports the hypothesis that LDM does indeed contain water ice (as already early hypothesized by, e.g., Kreslavsky & Head, 2002a). Small-scale polygons in Acidalia occur mostly at latitudes of $\sim 60\text{--}70^\circ\text{N}$, where LDM is prominent and near-surface ground ice should be stable under current conditions. According to the model of Chamberlain and Boynton (2007), the depth of ground ice is likely at ~ 10 cm around 63°N at current conditions, which is in good correlation with the concentration of small-scale polygons in Acidalia Planitia and in situ measurements of the Phoenix Lander mission (Mellon et al., 2008). This observation may support the hypothesis that the polygonal pattern is a result of thermal contraction cracking in regions with ice-cemented regolith. It does not, however, exclude a formation as desiccation cracks.

The bedrock distribution is anticorrelated to the LDM and shows that LDM is not a significant element of the landscape at latitudes equatorward of about 50°N (Figure 13m). However, the correlation of LDM and its degraded varieties (textured terrain; Figure 13b) with the GRS and model results is not perfect. Both LDM and textured terrain start already at $\sim 45^\circ\text{N}$, slightly south of the southern equilibrium boundary predicted by modeling. This may indicate that the current LDM was deposited in the past at higher (mean) obliquities ($25\text{--}30^\circ$; Chamberlain & Boynton, 2007), as already suggested by LDM dating (e.g., Willmes et al., 2012) and is currently degrading as indicated by its textured varieties and theoretically predicted by modeling (Schorghofer & Forget, 2012). The persistence of LDM at latitudes between 45°N and $50\text{--}55^\circ\text{N}$, where it is not dominant, would therefore be a remnant of a formerly more dominant LDM that is now not in equilibrium with environmental conditions. The presence of scalloped terrain at the very latitude where LDM and textured terrain become dominant supports this view. Scalloped terrain is thought to be a thermokarst landform resulting from sublimation (Dundas, 2017) and by definition requires a certain minimum thickness of LDM and/or textured terrain to develop. During the present period of LDM degradation at a phase of relatively low mean obliquity after the end of an ice age (Smith et al., 2016), scalloped terrain would therefore be expected to occur at the southernmost extent of dominant LDM/textured terrain, as is indeed observed (Figure 13d). With further thermokarstic degradation of the LDM, the extent of scalloped terrain should move further northward as the stability of ice follows the tilt of the rotational axis (Chamberlain & Boynton, 2007). Individual scalloped depressions are smaller in Acidalia than in Utopia, which appears to be consistent with the observation that the southern boundary of LDM/textured terrain is located further north in Acidalia when compared to Utopia and Arcadia Planitiae. This shift in LDM extent may suggest a less extended and possibly thinner LDM in Acidalia, and consequently a smaller dimension of scalloped depressions, as observed.

4.3. Small Pits on Equator-Facing Slopes

Small pits are mostly located in the southern parts of the mapping area, immediately north of the dichotomy boundary between the southern highlands and the northern lowlands (approximately 24°N to 34°N ; Figure 13f). The landscape is characterized by relatively smooth plains (Figure 2b), and no traces of the LDM and its degraded varieties are observed at such southern latitudes. Although the pits are partly filled by aeolian bedforms, indicating that pit formation was not the latest geological event in that region, they appear to be relatively young based on their pristine morphology and the lack of small impact craters in their interiors.

The raised rims suggest that either the negative topographic landforms were excavated by a high-energy process that threw out material or that material accumulated around or embayed a former positive topographic landform that has now disappeared (relief inversion). Alternatively, the raised rims would imply the collapse of pingos. Pingos are massive ice cored mounds, which develop through pressurized groundwater flow, progressive freezing mechanisms, and updoming of the surface in terrestrial periglacial environments (Hauber et al., 2011; Mackay, 1988; Wu et al., 2005). The hydraulic (open) system pingos (OSP) derive their water pressure from a topographic (hydraulic) gradient (Hauber et al., 2011; Wu et al., 2005). The recharge zone of the groundwater flow is located in topographic heights and the discharge zone is usually in the topographic lows. The groundwater flows through the subpermafrost or intrapermafrost aquifers. During continuous and slow water supply, high pressure builds up under the frozen surface layer at the topographical low area. The water injects into the frozen layer and the ice core of the pingo starts to grow, which can take centuries to form. OSP occur in clusters on river deltas, alluvium of valley bottoms or alluvial fans (Hauber et al., 2011; Mackay, 1988) and show an oval or oblong shape. During the growth of a pingo, dilation cracks form due to the increasing tension and the width of these cracks develops over time and exposes the ice core of the pingo. As the result of the exposure, the ice core will consequently melt away, and this process leads to the collapse of the pingo. The residual landform exhibits a raised rim compared to the surrounding topography (Mackay, 1988). Possible OSP were described in and around the Argyre basin at the midlatitudes of Mars (Soare, Conway, Dohm, & El-Maarry, 2014). The shape of mounds ranges from circular to elongate and are subkilometer in diameter. They occur in both sparse and dense clusters in different locations such as on the inner crater walls or on crater floors together with gullies (Soare, Conway, Dohm, & El-Maarry, 2014). Both the pingo candidates and pits are similar in size and morphology along with the occurrence of landforms on the inner crater walls. However, pingos do not show a “nested” appearance on the steepest slopes of the inner crater walls, unlike the pits. In contrast to the strong orientation dependence of equator-facing pits, there is no reported orientation preference for pingos in Argyre basin. Furthermore, pits do not occur together with gullies in Acidalia Planitia. In any case, the raised rims rule out a formation by simple collapse.

The preferential location of small pits on equator-facing slopes and their sometimes very irregular plan view shapes argues against a formation as primary or secondary craters. Similarly, an igneous volcanic origin (as speculated by Martínez-Alonso et al., 2011) appears unlikely, as there would be little reason to expect an insolation control on volcanic vents.

It has been suggested that these pits formed as blowouts in response to unidirectional winds (Kuznetsov et al., 2005). A blowout is a saucer-, cup- or trough-shaped hollow formed by wind erosion on a sand deposit, usually as a result of a loss of vegetation (Hesp, 2002). Blowouts on Earth are commonly observed in coastal environments but are also known from dunes in cold climates (Dijkmans & Koster, 1990). However, although aeolian bedforms are abundant in and around the pits, an erosional formation as blowouts appears unlikely, as the high amount of boulder-sized blocks is not consistent with a dune-like substrate. Moreover, it is impossible that boulder-sized objects, which could not be resolved in the images available to Kuznetsov et al. (2005), were displaced by wind. A control by unidirectional winds blowing in southwesterly directions, as proposed by Kuznetsov et al. (2005) on the basis of wind streaks orientation in the lee of craters, is inconsistent with the location of pit clusters on slopes with different aspects (Figure 7b). We therefore conclude that aeolian processes were not the main responsible mechanism for pit formation.

The preferential location of the pits on equator-facing slopes strongly suggests a control by insolation. One possibility would be a formation that is somehow linked to water ice. Although there is no currently observable trace of LDM at the locations of the pits, water ice may have been present at these latitudes in the past. Mars Odyssey Neutron Spectrometer Water Equivalent Hydrogen (WEH) maps show near-surface water ice at low latitudes between 20°N and 30°N (Pathare et al., 2018; Wilson et al., 2018), and there is evidence for past and present water ice deposits equatorward of 30°N (e.g., Hauber et al., 2008; Head et al., 2005; Vincendon et al., 2010). The WEH map (Wilson et al., 2018) shows <10% of water at the latitude range of the pits, suggesting that LDM or other types of water ice deposits may have extended that far south (Figures 14d and supporting information S3).

The morphology of some pits, especially the downslope margins, resembles that of glacial moraines (Figure 7). Sublimation of glacial ice (e.g., as *dry* ablation hollows; Mangold, 2011) would indeed leave a

rimmed depression, but only if some material had accumulated along the ice margins, for example, as ice-sediment contact or drop moraines at the margins of cold-based glaciers (Atkins, 2013). If there was ever any glacial ice, it would probably have been cold based as no proglacial or glaciofluvial features such as channels or eskers (Fassett et al., 2010; Gallagher & Balme, 2015) were observed. A repeated sequence of past ice accumulation and sublimation could explain the *nested* occurrence of pits (Figure 7a). However, the very small sizes of the depressions would imply numerous very small glaciers next to each other (Figure 9a). It is not clear either how sediment would have accumulated all around them, without an obvious source of boulder-sized sediments (e.g., Figure 8a).

If the pits were related to subsurface ice lenses or other forms of excess ice instead of glaciers, then the ice may have been precipitated during periods of high obliquity (above 45°; Forget et al., 2006) and sublimated at periods of low obliquity (below 25°) from the equatorial and midlatitudinal regions (Levrard et al., 2004). However, a formation by sublimation of water ice and thermokarstic collapse is unlikely, as it would not fully explain the irregular-shaped raised rims of the pits.

Another, more speculative hypothesis would be a dynamic scenario of CO₂ ice, or clathrate hydrate destabilization. For example, downslope transport of sediment deposited above sublimating slabs of CO₂ ice was modeled by Cedillo-Flores et al. (2011), who found that loose sediment can be fluidized. However, the model only accounted for fluidization of thin layers of sand and dust ($\ll 1$ m) mostly in polar regions and does not seem applicable for meter-sized boulders at latitudes equatorward of 30°N. Another scenario was proposed by Kieffer (2000a) and Kieffer et al. (2006) to explain the formation of dark splotches in the south polar region during the retreat of seasonal CO₂ ice in spring and summer. Warming of the regolith by insolation causes some CO₂ ice at the bottom of the slab to sublimate, building up gas pressure that eventually ruptures the slab and causes an eruptive jet of CO₂ gas and regolith material. If the proportion of regolith material in the jets is large enough, such an *explosive* mechanism may account for raised rims around a depression, analogous to an explosive volcanic eruption building a scoria or tuff cone. In an attempt to explain gully formation without liquid water, Pilorget and Forget (2016) examined the possibility of mobilizing regolith that is sandwiched between ice-cemented, impermeable permafrost at depth and a slab of translucent CO₂ ice on top. When the regolith is heated by insolation in spring, CO₂ ice at the bottom of the slab sublimates, the gas pressure can be high enough to crack the slab. The gas pressure is suddenly released and a jet of CO₂ gas can eject solid regolith material. This type of process would explain the control by insolation, large boulders, and the raised rims; however, at none of the modeled obliquities (25.2° and 35.2°) would this type of activity be expected at equator-facing scarps. As no CO₂ ice has yet been observed at the low latitudes at which the pits are located (Vincendon, 2015), models of pit formation involving solid state CO₂ are difficult to reconcile with the present climate of Mars and do not seem to apply at the latitudes at which the pits are observed. On the other hand, very cold surface areas might cause occasionally CO₂ condensation even close to the equator (Piqueux et al., 2016). If CO₂ accumulation was much higher at some time in the recent past at latitudes $< 30^\circ\text{N}$, it may have been linked to formation of pits. Alternatively, dissociation of clathrate hydrates (methane [CH₄·*n*H₂O] or CO₂ [CO₂·*n*H₂O]) could perhaps trigger an energetic release of volatiles. On Earth, violent gas blowouts have created craters with raised ejecta rims on the Yamal peninsula in Russia (e.g., Buldovich et al., 2018; Leibman et al., 2014), and subaqueous craters in the Arctic were formed by massive release of methane from destabilized gas hydrates (Andreassen et al., 2017). Methane has been detected in the Martian atmosphere (Webster et al., 2018), and may have been present in the past as well. Thermodynamic calculations predict the past and perhaps present formation of methane clathrate at the base of the cryosphere at depths of a few kilometers, and at the surface or in the shallow subsurface down to a few meters at past periods of higher atmospheric (and methane partial) pressure (Mousis et al., 2013). While the most plausible location of Martian clathrates would be the cold polar regions (the formation requires temperatures down to ~ 150 K), metastable clathrates could even be present at lower latitudes than thermodynamic models suggest (Mousis et al., 2013). The release of metastable methane clathrate particles (i.e., not gaseous CH₄) has been proposed to account for the methane in the Martian atmosphere (Chassefière, 2009). It was also speculated that methanogenic explosions were responsible for the origin of thousands of small cratered mounds in Elysium Planitia on Mars (Page, 2018).

The small pits are located in a latitude range that partly overlaps the TPT and with SPM, and which has its northern margin approximately where LPM and kilometer-scale polygons begin (Figure 13). Most of these

landforms have been associated with some sort of subsurface sediment mobilization and volatile release (e.g., Allen et al., 2013; Etiope et al., 2011; Farrand et al., 2005; Hemmi & Miyamoto, 2018; Oehler & Allen, 2010; Oehler & Etiope, 2017; Salvatore & Christensen, 2014; Skinner & Mazzini, 2009). In this respect, it may be speculated that there is a whole spatially contiguous series landforms related to subsurface volatile release which consists, from north to south, of kilometer-scale polygons and LPM, SPM, TPT, and small pits. If this is true, a local control of methane release by enhanced insolation might explain the control of slope aspect (orientation) on pit location (Figures 7–9). Indeed, obliquity (insolation) variations were proposed to be a triggering factor in possible methane clathrate destabilization on Mars (Kite et al., 2017; Root & Elwood Madden, 2012). The spatial alignment of many small pits along topographic ridges (Figure 9) may be explained by a control of vent locations by fractures beneath the ridges, which would provide pathways for ascending volatiles if these were deep-seated. Deeply rooted fractures would not, however, account for pit locations in south facing crater walls (Figure 7), so postimpact shallow methane clathrates (rather than deep ones) would seem more likely in the craters.

It has been hypothesized that methane clathrate hydrates might have been destabilized in the interglacial starting at 0.4 Ma (Prieto-Ballesteros et al., 2006), when a confining ice layer retreated poleward and reduced the pressure in a zone of clathrate stability. Such a scenario would be consistent with the apparent young age of the pits. Nevertheless, it needs to be emphasized that evidence for low-latitude methane clathrate hydrate deposits, either deeply seated or in the near subsurface, is still missing, and at last for the latter it is unclear if they could ever have formed in the respective climatic conditions (Falenty & Kuhs, 2007; Kieffer, 2000b; Kuhs & Klapproth, 2000).

In summary, the enigmatic pits were only observed in Chryse/Acidalia Planitiae in our mapping studies (Ramsdale et al., 2018; Séjourné et al., 2018) and are very rare elsewhere (Kuznetsov et al., 2005), thus we suggest that specific conditions in southern Acidalia Planitia, perhaps related to the accumulation of large amounts of fine-grained volatile-rich sediments, favor their origin. They may belong to a suite of landforms that may all be related to volatile release, and their specific locations are locally controlled by slope aspect (orientation). The raised and irregular-shaped morphology suggests an energetic release of volatiles, although the mechanism remains unclear.

5. Conclusion

We performed the first contiguous regional mapping of selected ice- and water-related landforms at full CTX resolution along a 300-km-wide strip in Acidalia Planitia, from 20°N to 84°N latitude. Our mapping of Acidalia Planitia is part of a joint effort to study the three main basins of the northern lowlands: Acidalia, Utopia, and Arcadia Planitiae. We used a grid-mapping technique (Ramsdale et al., 2017; Voelker et al., 2017) to analyze the distribution of 13 types of possibly volatile-related landforms. This technique has proven to be very effective to map small-scale features over very large areas. Our results show a similar pattern of landform distribution as previous studies of individual landforms, but there are significantly more details in the present study using the high-resolution grid-mapping technique.

Our mapping identified four assemblages of landforms based on their distribution, spatial association at small scale and correlation to various data sets:

- (1) Geologically recent polar cap (massive ice)
- (2) Possible water-related features (kilometer-scale polygons, LPM, SPM, and TPT)
- (3) Ice-related landforms, such as geologically young LDM, textured terrain, small-scale polygons, scalloped terrain, gullies, and large-scale VFF.
- (4) Irregular-shaped, equator-facing pits with a hypothesized origin by energetic release of volatiles or mantle degradation. These features have never been described in detail before on the basis of very high resolution images.

LDM and textured terrain occur ubiquitously from 44°N to 78°N in Acidalia Planitia further north than in Arcadia and Utopia Planitiae (Ramsdale et al., 2018; Séjourné et al., 2018). The origin of ice by air fall deposition is most likely, as LDM and its degraded varieties are draped over the terrain regardless of topography and are uncorrelated with geologic boundaries, outflow channels, or tectonic features, as would be expected if the ice had a fluvial or groundwater origin. This finding is consistent with climatic models (e.g.,

Chamberlain & Boynton, 2007; Mellon & Jakosky, 1995) predicting current ice stability down to 50°N. Moreover, models of WEH distribution show <10% of hydrogen far southward than the present distribution of LDM, suggesting that ice might have been formerly present at latitudes lower than 50°N.

Degradation and modification of the LDM results in textured terrain (from 36°N–43°N to 79°N), scalloped terrain (46°N–57°N), gullies (32°N–53°N), and small-scale polygons (51°N–74°N). These landforms provide evidence for ice loss and thermal contraction between 32°N and 79°N in Acidalia Planitia, and overlap spatially with LDM from about 40–44°N to 78°N. Based on models of WEH soil content and the lack of SHARAD detections, Acidalia Planitia appears to have less ice in the uppermost tens of meters than Arcadia or Utopia Planitiae. This finding suggests either past or current differences among the main basins in the northern lowlands with respect to climatic conditions.

In the south of the mapping area, a suite of landforms (kilometer-scale polygons, large and pitted mounds, and the so-called thumbprint terrain), is possibly related to the existence of originally volatile-rich, fine-grained sediment and its later subsurface remobilization and outgassing.

The origin of small, irregular-shaped pits with raised rims on mostly, equator-facing slopes in the southernmost portion of the strip is enigmatic. They form a spatial continuum with the landforms that are possibly related to sediment reworking, but are likely much younger. Whatever their exact formation mechanism, they are likely the result of an energetic release of volatiles (H₂O, CO₂, CH₄), rather than impact-, volcanism-, or wind-related processes.

A forthcoming synthesis of the three studied strips across Acidalia, Utopia, and Arcadia Planitiae, which are thought to be representative of the whole northern lowlands, will enable identifying key locations to link the investigated areas. Moreover, we suggest that the grid-mapping technique will be a useful tool to constrain the large-scale distribution of small-scale hazards (e.g., aeolian landforms) and features with high scientific potential (e.g., mineral filling veins, fractures) at landing sites for future planetary missions.

Acknowledgments

This work is a joint effort of an International Team sponsored by the International Space Science Institute (ISSI) in Bern (CH). It was further supported by the German Aerospace Center (DLR) in Berlin Adlershof and the Planetary Sciences and Remote Sensing Group of the Department of Earth Sciences at the Freie Universität Berlin (FUB). A. Losiak was supported by the National Science Centre Poland (Narodowe Centrum Nauki) grant UMO-2013/08/S/ST10/00586. We are also grateful to Jay Dickson and an anonymous reviewer for their detailed and constructive comments. We thank the CTX camera team for their successful planning and acquisition of the data. We would like to thank Caleb I. Fassett for his helpful comments and discussions. The derived data products are available at FUB data repository (http://www.planet.geo.fu-berlin.de/Orgel_etal_2018_Acidalia_Planitia.zip) as supporting information.

References

- Aharonson, O., & Schorghofer, N. (2006). Subsurface ice on Mars with rough topography. *Journal of Geophysical Research*, *111*, E11007. <https://doi.org/10.1029/2005JE002636>
- Albee, A. L., Palluconi, F. D., & Arvidson, R. E. (1998). Mars global surveyor mission: Overview and status. *Science*, *279*(5357), 1671–1672. <https://doi.org/10.1126/science.279.5357.1671>
- Allen, C. C., Oehler, D. Z., Etiope, G., van Rensbergen, P., Baciu, C., Feyzullayev, A., et al. (2013). Fluid expulsion in terrestrial sedimentary basins: A process providing potential analogs for giant polygons and mounds in the martian lowlands. *Icarus*, *224*(2), 424–432. <https://doi.org/10.1016/j.icarus.2012.09.018>
- Andreassen, A., Hubbard, A., Winsborrow, M., Patton, H., Vadakkepullyambatta, S., Plaza-Faverola, A., et al. (2017). Massive blow-out craters formed by hydrate-controlled methane expulsion from the Arctic seafloor. *Science*, *356*(6341), 948–953. <https://doi.org/10.1126/science.aal4500>
- Atkins, C. B. (2013). Geomorphological evidence for cold-based glacier activity in South Victoria Land, Antarctica. In M. J. Hambrey, et al. (Eds.), *Antarctic paleoenvironments and Earth-surface processes*. *Geological Society London, Special Publications*, *381*, 299–318. <https://doi.org/10.1144/SP381.18>
- Balme, M. R., Mangold, N., Baratoux, D., Costard, F., Gosselin, M., Masson, P., et al. (2006). Orientation and distribution of recent gullies in the southern hemisphere of Mars: Observations from high resolution stereo camera/Mars express (HRSC/MEX) and Mars orbiter camera/Mars global surveyor (MOC/MGS) data. *Journal of Geophysical Research*, *111*, E05001. <https://doi.org/10.1029/2005JE002607>
- Berndt, C., Jacobs, C., Evans, A., Elliott, A. G. G., Long, D., & Hitchen, K. (2012). Kilometre-scale polygonal seabed depressions in the Hatton Basin, NE Atlantic Ocean: Constraints on the origin of polygonal faulting. *Marine Geology*, *332*–334, 126–133.
- Bishop, M. P., James, L. A., Schroder, J. F., & Walsh, S. J. (2012). Geospatial technologies and digital geomorphological mapping: Concepts, issues and research. *Geomorphology*, *137*(1), 5–26. <https://doi.org/10.1016/j.geomorph.2011.06.027>
- Boynton, W. V., Feldman, W. C., Squyres, S. W., Prettyman, T. H., Brückner, J., Evans, L. G., et al. (2002). Distribution of hydrogen in the near surface of Mars: Evidence for subsurface ice deposits. *Science*, *297*(5578), 81–85. <https://doi.org/10.1126/science.1073722>
- Bramson, A. M., Byrne, S., & Bapst, J. (2017). Preservation of mid-latitude ice sheets on Mars. *Journal of Geophysical Research: Planets*, *122*, 2250–2266. <https://doi.org/10.1002/2017JE005357>
- Bramson, A. M., Byrne, S., Putzig, N. E., Sutton, S., Plaut, J. J., Brothers, T. C., et al. (2015). Widespread excess ice in Arcadia Planitia, Mars. *Geophysical Research Letters*, *42*, 6566–6574. <https://doi.org/10.1002/2015GL064844>
- Bridges, J. C., Seabrook, A. M., Rothery, D. A., Kim, J. R., Pillinger, C. T., Sims, M. R., et al. (2003). Selection of the landing site in Isidis Planitia of Mars probe Beagle 2. *Journal of Geophysical Research*, *108*(E1), 5001. <https://doi.org/10.1029/2001JE001820>
- Bridges, N. T., & Lackner, C. N. (2006). Northern hemisphere Martian gullies and mantled terrain: Implications for near-surface water migration in Mars' recent past. *Journal of Geophysical Research*, *111*, E09014. <https://doi.org/10.1029/2006JE002702>
- Bruno, B. C., Fagents, S. A., Thordarson, T., Baloga, S. M., & Pilger, E. (2004). Clustering within rootless cone groups on Iceland and Mars: Effect of nonrandom processes. *Journal of Geophysical Research*, *109*, E07009. <https://doi.org/10.1029/2004JE002273>
- Buczkowski, D. L., Seelos, K. D., & Cooke, M. L. (2012). Giant polygons and circular graben in western Utopia basin, Mars: Exploring possible formation mechanisms. *Journal of Geophysical Research*, *117*, E08010. <https://doi.org/10.1029/2011JE003934>
- Buldovich, S., Khilimonyuk, V., Bychkov, A., Ospennikov, E., Vorobyev, S., Gunar, A., et al. (2018). Cryogenic hypothesis of the Yamal crater origin: Results of detailed studies and modeling. In P. Deline, X. Bodin, & L. Ravanel (Eds.), *5th European Conference on Permafrost – Book of Abstracts* (pp. 97–98). France: Chamonix.

- Byrne, S., Dundas, C. M., Kennedy, M. R., Mellon, M. T., McEwen, A. S., Cull, S. C., et al. (2009). Distribution of mid-latitude ground ice on Mars from new impact craters. *Science*, 325(5948), 1674–1676. <https://doi.org/10.1126/science.1175307>
- Campbell, B. A., Schroeder, D. M., & Whitten, J. L. (2018). Mars radar clutter and surface roughness characteristics from MARSIS data. *Icarus*, 299, 22–30. <https://doi.org/10.1016/j.icarus.2017.07.011>
- Canzler, L.P. (2014). Geologic map of gullies and cold-climate landforms in Acidalia Mensa, Mars. Bachelor-thesis, Westfälische Wilhelms-Universität Münster, p. 59.
- Cedillo-Flores, Y., Treiman, A. H., Lasue, J., & Clifford, S. M. (2011). CO₂ gas fluidization in the initiation and formation of Martian polar gullies. *Geophysical Research Letters*, 38, L21202. <https://doi.org/10.1029/2011GL049403>
- Chamberlain, M. A., & Boynton, W. V. (2007). Response of Martian ground ice to orbit-induced climate change. *Journal of Geophysical Research*, 112, E06009. <https://doi.org/10.1029/2006JE002801>
- Chassefière, E. (2009). Metastable methane clathrate particles as a source of methane to the Martian atmosphere. *Icarus*, 204(1), 137–144. <https://doi.org/10.1016/j.icarus.2009.06.016>
- Christensen, P. R. (2003). Formation of recent Martian gullies through melting of extensive water-rich snow deposits. *Nature*, 422(6927), 45–48. <https://doi.org/10.1038/nature01436>
- Conway, S. J., & Balme, M. R. (2014). Decameter thick remnant glacial ice deposits on Mars. *Geophysical Research Letters*, 41, 5402–5409. <https://doi.org/10.1002/2014GL060314>
- Conway, S. J., Hovius, N., Barnie, T., Besserer, J., Le Mouélic, S., Orosei, R., et al. (2012). Climate-driven deposition of water ice and the formation of mounds in craters in Mars' north polar region. *Icarus*, 220, 174–193. <https://doi.org/10.1016/j.icarus.2012.04.021>
- Costard, F., Forget, F., Mangold, N., & Peulvast, J. P. (2002). Formation of recent Martian debris flows by melting of near-surface ground ice at high obliquity. *Science*, 295(5552), 110–113. <https://doi.org/10.1126/science.1066698>
- Costard, F. M., & Kargel, J. S. (1995). Outwash plains and thermokarst on Mars. *Icarus*, 114(1), 93–112. <https://doi.org/10.1006/icar.1995.1046>
- Davis, P. A., & Tanaka, K. L. (1995). Curvilinear ridges in Isidis Planitia, Mars—The result of mud volcanism? 26th Lunar and Planetary Science Conference, Houston, TX, pp. 321–322.
- Decker, M. (2015). Geologic map of gullies and cold-climate landforms in Acidalia Colles, Mars. Bachelor-thesis, Westfälische Wilhelms-Universität Münster, p. 38.
- Dickson, J. L., Head, J. W., Goudge, T. A., & Barbieri, L. (2015). Recent climate cycles on Mars: Stratigraphic relationships between multiple generations of gullies and the latitude dependent mantle. *Icarus*, 252, 83–94. <https://doi.org/10.1016/j.icarus.2014.12.035>
- Dickson, J. L., Head, J. W., & Kreslavsky, M. (2007). Martian gullies in the southern mid-latitudes of Mars: Evidence for climate-controlled formation of young fluvial features based upon local and global topography. *Icarus*, 188(2), 315–323. <https://doi.org/10.1016/j.icarus.2006.11.020>
- Dijkmans, J. W. A., & Koster, E. A. (1990). Morphological development of dunes in a subarctic environment, Central Kobuk Valley, north-western Alaska. *Geografiska Annaler. Series A, Physical Geography*, 72(1), 93–109. <https://doi.org/10.1080/04353676.1990.11880303>
- Dundas, C. M. (2017). Effects of varying obliquity on Martian sublimation thermokarst landforms. *Icarus*, 281, 115–120. <https://doi.org/10.1016/j.icarus.2016.08.031>
- Dundas, C. M., Bramson, A. M., Ojha, L., Wray, J. J., Mellon, M. T., Byrne, S., et al. (2018). Exposed subsurface ice sheets in the Martian mid-latitudes. *Science*, 359(6372), 199–201. <https://doi.org/10.1126/science.aao1619>
- Dundas, C. M., Byrne, S., & McEwen, A. S. (2015). Modeling the development of Martian sublimation thermokarst landforms. *Icarus*, 262, 154–169. <https://doi.org/10.1016/j.icarus.2015.07.033>
- Dundas, C. M., Byrne, S., McEwen, A. S., Mellon, M. T., Kennedy, M. R., Daubar, I. J., et al. (2014). HiRISE observations of new impact craters exposing Martian ground ice. *Journal of Geophysical Research: Planets*, 119, 109–127. <https://doi.org/10.1002/2013JE004482>
- Dundas, C. M., Diniega, S., & McEwen, A. S. (2015). Long-term monitoring of Martian gully formation and evolution with MRO/Hirise. *Icarus*, 251, 244–263. <https://doi.org/10.1016/j.icarus.2014.05.013>
- Dundas, C. M., McEwen, A. S., Diniega, S., Hansen, C. J., Byrne, S., & McElwaine, J. N. (2017). The formation of gullies on Mars today. In S. J. Conway, J. L. Carrivick, P. A. Carling, T. de Haas, & T. N. Harrison (Eds.), *Martian gullies and their earth analogues* (Vol. 467). London: Geological society, Special publications. <https://doi.org/10.1144/SP467.5>
- El Maarry, M. R., Markiewicz, W. J., Mellon, M. T., Goetz, W., Dohm, J. M., & Pack, A. (2010). Crater floor polygons: Desiccation patterns of ancient lakes on Mars? *Journal of Geophysical Research*, 115, E10006. <https://doi.org/10.1029/2010JE003609>
- Etiopie, G., Oehler, D. Z., & Allen, C. C. (2011). Methane emissions from Earth's degassing: Implications for Mars. *Planetary and Space Science*, 59(2–3), 182–195. <https://doi.org/10.1016/j.pss.2010.06.003>
- Falenty, A., & Kuhs, W. F. (2007). Laboratory study on the kinetics of CO₂ hydrates in a broad p-T range relevant to Mars. EPSC abstracts, Vol. 2, EPSC2007-A-00363 (<https://www.cosis.net/abstracts/EPSC2007/00363/EPSC2007-J-00363.pdf>).
- Farrand, W. H., Gaddis, L. R., & Keszthelyi, L. (2005). Pitted cones and domes on Mars: Observations in Acidalia Planitia and Cydonia Mensae using MOC, THEMIS, and TES data. *Journal of Geophysical Research*, 110, E05005. <https://doi.org/10.1029/2004JE002297>
- Fassett, C. I., Dickson, J. L., Head, J. W., Levy, J. S., & Marchant, D. R. (2010). Supraglacial and proglacial valleys on Amazonian Mars. *Icarus*, 208(1), 86–100. <https://doi.org/10.1016/j.icarus.2010.02.021>
- Fassett, C. I., Levy, J. S., Head, J. W., & Dickson, J. L. (2014). An extended period of episodic northern and mid-latitude glaciation on Mars during the mid-to-late Amazonian: Implications for long-term obliquity history. *Geology*, 42(9), 763–766. <https://doi.org/10.1130/G35798.1>
- Feldman, W. C., Prettyman, T. H., Maurice, S., Plaut, J. J., Bish, D. L., Vaniman, D. T., et al. (2004). Global distribution of near-surface hydrogen on Mars. *Journal of Geophysical Research*, 109, E09006. <https://doi.org/10.1029/2003JE002160>
- Forget, F., Byrne, S., Head, J. W., Mischna, M. A., & Schörghofer, N. (2017). Recent climate variations. In R. M. Haberle, et al. (Eds.), *The atmosphere and climate of Mars* (pp. 497–525). Cambridge, UK: Cambridge University Press.
- Forget, F., Haberle, R. M., Montmessin, F., Levrard, B., & Head, J. W. III (2006). Formation of glaciers on Mars by atmospheric precipitation at high obliquity. *Science*, 311(5759), 368–371. <https://doi.org/10.1126/science.1120335>
- Frigge, M., Hoaglin, D. C., & Iglewicz, B. (1989). Some implementations of the boxplot. *The American Statistician*, 43(1), 50–54.
- Gallagher, C., & Balme, M. (2015). Eskers in a complete, wet-based glacial system in the Phlegra Montes region, Mars. *Earth and Planetary Science Letters*, 431, 96–109. <https://doi.org/10.1016/j.epsl.2015.09.023>
- Gallagher, C., Balme, M., Soare, R., & Conway, S. J. (2018). Formation and degradation of chaotic terrain in the Galaxias regions of Mars: Implications for near-surface storage of ice. *Icarus*, 309, 69–83. <https://doi.org/10.1016/j.icarus.2018.03.002>
- Ghent, R. R., Anderson, S. W., & Pithawala, T. M. (2012). The formation of small cones in Isidis Planitia, Mars through mobilization of pyroclastic surge deposits. *Icarus*, 217(1), 169–183. <https://doi.org/10.1016/j.icarus.2011.10.018>
- Greenlee, R., & Guest, J. E. (1987). Geologic map of the eastern equatorial region of Mars: U.S. Geological Survey miscellaneous investigations series Map I–1802–B, scale 1:15,000,000.

- Grizzaffi, P., & Schultz, P. H. (1989). Isidis basin: Site of ancient volatile-rich debris layer. *Icarus*, 77, 358–381.
- Harrison, T. N., Osinski, G. R., Tornabene, L. L., & Jones, E. (2015). Global documentation of gullies with the Mars reconnaissance orbiter context camera and implications for their formation. *Icarus*, 252, 236–254. <https://doi.org/10.1016/j.icarus.2015.01.022>
- Hauber, E., Reiss, D., Ulrich, M., Preusker, F., Trauthan, F., Zanetti, M., et al. (2011). Periglacial landscapes on Svalbard: Terrestrial analogs for cold-climate landforms on Mars. *Geological Society of America Special Papers*, 483, 177–201. [https://doi.org/10.1130/2011.2483\(12\)](https://doi.org/10.1130/2011.2483(12))
- Hauber, E., van Gasselt, S., Chapman, M. G., & Neukum, G. (2008). Geomorphic evidence for former lobate debris aprons at low latitudes on Mars: Indicators of the Martian paleoclimate. *Journal of Geophysical Research*, 113, E02007. <https://doi.org/10.1029/2007JE002897>
- Head, J. W. III, Marchant, D. R., Agnew, M. C., Fassett, C. I., & Kreslavsky, M. A. (2006). Extensive valley glacier deposits in the northern mid-latitudes of Mars: Evidence for late Amazonian obliquity-driven climate change. *Earth and Planetary Science Letters*, 241(3–4), 663–671. <https://doi.org/10.1016/j.epsl.2005.11.016>
- Head, J. W. III, Nahm, A. L., Marchant, D. R., & Neukum, G. (2006). Modification of the dichotomy boundary on Mars by Amazonian mid-latitude regional glaciation. *Geophysical Research Letters*, 33, L08S03. <https://doi.org/10.1029/2005GL024360>
- Head, J. W., Mustard, J. F., Kreslavsky, M., Milliken, R. E., & Marchant, D. R. (2003). Recent ice ages on Mars. *Nature*, 426, 797–802.
- Head, J. W., Neukum, G., Jaumann, R., Hiesinger, H., Hauber, E., Carr, M., et al., & the HRSC Co-Investigator Team (2005). Tropical to mid-latitude snow and ice accumulation, flow and glaciation on Mars. *Nature*, 434(7031), 346–351. <https://doi.org/10.1038/nature03359>
- Heldmann, J. L., Carlsson, E., Johansson, H., Mellon, M. T., & Toon, O. B. (2007). Observations of Martian gullies and constraints on potential formation mechanisms II. The northern hemisphere. *Icarus*, 188(2), 324–344. <https://doi.org/10.1016/j.icarus.2006.12.010>
- Hemmi, R., & Miyamoto, H. (2018). High-resolution topographic analyses of mounds in southern Acidalia Planitia, Mars: Implications for possible mud volcanism in submarine and subaerial environments. *Geosciences*, 8(5), 152. <https://doi.org/10.3390/geosciences8050152>
- Hesp, P. (2002). Foredunes and blowouts: Initiation, geomorphology and dynamics. *Geomorphology*, 48(1–3), 245–268. [https://doi.org/10.1016/S0169-555X\(02\)00184-8](https://doi.org/10.1016/S0169-555X(02)00184-8)
- Hiesinger, H., & Head, J. W. (2000). Characteristics and origin of polygonal terrain in southern Utopia Planitia, Mars: Results from Mars orbiter laser altimeter and Mars orbiter camera data. *Journal of Geophysical Research*, 105(E5), 11,999–12,022.
- Holt, J. W., Safaeinili, A., Plaut, J., Head, J. W. III, Phillips, R. J., Seu, R., et al. (2008). Radar sounding evidence for buried glaciers in the southern mid-latitudes of Mars. *Science*, 322(5905), 1235–1238. <https://doi.org/10.1126/science.1164246>
- Hubbard, B., Souness, C., & Brough, S. (2014). Glacier-like forms on Mars. *The Cryosphere*, 8(6), 2047–2061. <https://doi.org/10.5194/tc-8-2047-2014>
- Ivanov, M. A., Hiesinger, H., Erkeling, G., & Reiss, D. (2014). Mud volcanism and morphology of impact craters in Utopia Planitia on Mars: Evidence for the ancient ocean. *Icarus*, 228, 121–140. <https://doi.org/10.1016/j.icarus.2013.09.018>
- Ivanov, M. A., Hiesinger, H., Erkeling, G., & Reiss, D. (2015). Evidence for large reservoirs of water/mud in Utopia and Acidalia Planitiae on Mars. *Icarus*, 248, 383–391. <https://doi.org/10.1016/j.icarus.2014.11.013>
- Jakosky, B. M., Mellon, M. T., Varnes, E. S., Feldman, W. C., Boynton, W. V., & Haberle, R. M. (2005). Mars low-latitude neutron distribution: Possible remnant near-surface water ice and a mechanism for its recent emplacement. *Icarus*, 175, 58–67. <https://doi.org/10.1016/j.icarus.2004.11.014>
- Kadish, S. J., Barlow, N. G., & Head, J. W. (2009). Latitude dependence of Martian pedestal craters: Evidence for a sublimation-driven formation mechanism. *Journal of Geophysical Research*, 114, E10001. <https://doi.org/10.1029/2008JE003318>
- Kargel, J. S., Baker, V. R., Begét, J. E., Lockwood, J. F., Péwé, T. L., Shaw, J. S., et al. (1995). Evidence of ancient continental glaciation in the Martian northern plains. *Journal of Geophysical Research*, 100(E3), 5351–5368. <https://doi.org/10.1029/94JE02447>
- Kieffer, H. H. (2000a). Annual punctuated CO₂ slab-ice and jets on Mars. Paper presented at the 2nd international conference on Mars polar science and exploration, University of Iceland, Reykjavik, abstract 4095.
- Kieffer, H. H. (2000b). Clathrates are not the culprit. *Science*, 287(5459), 1753b–11753b. <https://doi.org/10.1126/science.287.5459.1753b>
- Kieffer, H. H., Christensen, P. R., & Titus, T. N. (2006). CO₂ jets formed by sublimation beneath translucent slab ice in Mars' seasonal south polar ice cap. *Nature*, 442(7104), 793–796. <https://doi.org/10.1038/nature04945>
- Kite, E. S., Gao, P., Goldblatt, C., Mischna, M. A., Mayer, S. P., & Yung, Y. L. (2017). Methane bursts as a trigger for intermittent lake-forming climates on post-Noachian Mars. *Nature Geoscience*, 10, 737–740. <https://doi.org/10.1038/ngeo3033>
- Kneissl, T., Reiss, D., van Gasselt, S., & Neukum, G. (2010). Distribution and orientation of northern-hemisphere gullies on Mars from the evaluation of HRSC and MOC-NA data. *Earth and Planetary Science Letters*, 294(3–4), 357–367. <https://doi.org/10.1016/j.epsl.2009.05.018>
- Kostama, V. P., Kreslavsky, M. A., & Head, J. W. III (2006). Recent high-latitude icy mantle in the northern plain of Mars: Characteristics and ages of emplacement. *Geophysical Research Letters*, 33, L11201. <https://doi.org/10.1029/2006GL025946>
- Kreslavsky, M. A., & Head, J. W. (2000). Kilometer-scale roughness of Mars' surface: Results from MOLA data analysis. *Journal of Geophysical Research*, 105(E11), 26,695–26,711. <https://doi.org/10.1029/2000JE001259>
- Kreslavsky, M. A., & Head, J. W. (2002a). Mars: Nature and evolution of young latitude-dependent water-ice-rich mantle. *Geophysical Research Letters*, 29(15), 1719. <https://doi.org/10.1029/2002GL015392>
- Kreslavsky, M. A., & Head, J. W. (2002b). Fate of outflow channel effluents in the northern lowlands of Mars: The Vastitas borealis formation as a sublimation residue from frozen ponded bodies of water. *Journal of Geophysical Research*, 107(E12), 5121. <https://doi.org/10.1029/2001JE001831>
- Kuhs, W. F., & Klapproth, A. (2000). CO₂ clathrate hydrates on Mars. Paper presented at the 2nd international conference on Mars polar science and exploration, University of Iceland, Reykjavik, abstract 4069.
- Kuznetsov, I. V., Kuzmin, R. O., & Greeley, R. (2005). Wind-related erosion depressions within a small impact craters in Chryse and Elysium Planitiae on Mars. 36th Lunar and Planetary Science Conference, Houston, TX, #1810.
- Lane, M. D., & Christensen, P. R. (2000). Convection in a catastrophic flood deposit as the mechanism for the giant polygons on Mars. *Journal of Geophysical Research*, 105(E7), 17,617–17,627. <https://doi.org/10.1029/1999JE001197>
- Laskar, J., Correia, A. C. M., Gastineau, M., Joutel, F., Levrard, B., & Robutel, P. (2004). Long term evolution and chaotic diffusion of the insolation quantities of Mars. *Icarus*, 170, 343–364.
- Lefort, A., Russell, P. S., & Thomas, N. (2010). Scalloped terrains in the Peneus and Amphitrites Paterae region of Mars as observed by HiRISE. *Icarus*, 205, 259–268.
- Lefort, A., Russell, P. S., Thomas, N., McEwen, A. S., Dundas, C. M., & Kirk, R. L. (2009). Observations of periglacial landforms in Utopia Planitia with the High Resolution Imaging Science Experiment (HiRISE). *Journal of Geophysical Research*, 114, E04005. <https://doi.org/10.1029/2008JE003264>
- Leibman, M. O., Kizyakov, A. I., Plekhanov, A. V., & Streletskaia, I. D. (2014). New permafrost feature—Deep crater in central Yamal (West Siberia, Russia) as a response to local climate fluctuations. *Geography, Environment, Sustainability*, 7(4), 68–79. <https://doi.org/10.24057/2071-9388-2014-7-4-68-79>

- Leverard, B., Forget, F., Montmessin, F., & Laskar, J. (2004). Recent ice-rich deposits formed at high latitudes on Mars by sublimation of unstable equatorial ice during low obliquity. *Nature*, *431*(7012), 1072–1075. <https://doi.org/10.1038/nature03055>
- Levy, J. S., Fassett, C. I., Head, J. W., Schwartz, C., & Watters, J. L. (2014). Sequestered glacial ice contribution to the global Martian water budget: Geometric constraints on the volume of remnant, mid-latitude debris-covered glaciers. *Journal of Geophysical Research: Planets*, *119*, 2188–2196. <https://doi.org/10.1002/2014JE004685>
- Levy, J. S., Head, J. W. III, & Marchant, D. R. (2009a). Thermal contraction crack polygons on Mars: Classification, distribution, and climate implications from HiRISE observations. *Journal of Geophysical Research*, *114*, E01007. <https://doi.org/10.1029/2008JE003273>
- Levy, J. S., Head, J. W. III, & Marchant, D. R. (2009b). Concentric crater fill in Utopia Planitia: History and interaction between glacial “brain terrain” and periglacial mantle processes. *Icarus*, *202*(2), 462–476. <https://doi.org/10.1016/j.icarus.2009.02.018>
- Levy, J. S., Marchant, D. R., & Head, J. W. III (2010). Thermal contraction crack polygons on Mars: A synthesis from HiRISE, Phoenix, and terrestrial analog studies. *Icarus*, *206*(1), 229–252. <https://doi.org/10.1016/j.icarus.2009.09.005>
- Lockwood, J. F., Kargel, J. S., & Strom, R. B. (1992). Thumbprint terrain on the northern plains: A glacial hypothesis. 28th Lunar and Planetary Science Conference, Houston, TX, #1395.
- Lucchitta, B. K. (1981). Mars and Earth: Comparison of cold-climate features. *Icarus*, *45*, 264–303.
- Lucchitta, B. K., Ferguson, H. M., & Summers, C. (1986). Sedimentary deposits in the northern lowland plains, Mars. *Journal of Geophysical Research*, *91*, E166–E174. <https://doi.org/10.1029/JB091iB13p0E166>
- Mackay, J. R. (1988). Pingo growth and collapse, Tuktoyaktuk peninsula area, Western Arctic coast, Canada: A long-term field study. *Géographie Physique et Quaternaire*, *52*, 271–323.
- Madeleine, J.-B., Head, J. W., Forget, F., Navarro, T., Millour, E., Spiga, A., et al. (2014). Recent ice ages on Mars: The role of radiatively active clouds and cloud microphysics. *Geophysical Research Letters*, *41*, 4873–4879. <https://doi.org/10.1002/2014GL059861>
- Malin, M. C., Bell, J. F., Cantor, B. A., Caplinger, M. A., Calvin, W. M., Clancy, R. T., et al. (2007). Context camera investigation on board the Mars reconnaissance orbiter. *Journal of Geophysical Research*, *112*, E05S04. <https://doi.org/10.1029/2006JE002808>
- Malin, M. C., & Edgett, K. S. (2000). Evidence for recent groundwater seepage and surface runoff on Mars. *Science*, *288*(5475), 2330–2335. <https://doi.org/10.1126/science.288.5475.2330>
- Mangold, N. (2005). High latitude patterned grounds on Mars: Classification, distribution and climatic control. *Icarus*, *174*(2), 336–359. <https://doi.org/10.1016/j.icarus.2004.07.030>
- Mangold, N. (2011). Ice sublimation as a geomorphic process: A planetary perspective. *Geomorphology*, *126*, 1–17.
- Marchant, D. R., & Head, J. W. III (2007). Antarctic dry valleys: Microclimate zonation, variable geomorphic processes, and implications for assessing climate change on Mars. *Icarus*, *192*(1), 187–222. <https://doi.org/10.1016/j.icarus.2007.06.018>
- Martinez-Alonso, S., Mellon, M. T., Banks, M. E., Keszhelyi, L. P., & McEwen, A. S. (2011). Evidence of volcanic and glacial activity in Chryse and Acidalia Planitiae. Mars. *Icarus*, *212*(2), 597–621. <https://doi.org/10.1016/j.icarus.2011.01.004>
- McEwen, A. S., Banks, M. E., Baugh, N., Becker, K., Boyd, A., Bergstrom, J. W., et al. (2010). The High Resolution Imaging Science Experiment (HiRISE) during MRO's primary science phase (PSP). *Icarus*, *205*(1), 2–37. <https://doi.org/10.1016/j.icarus.2009.04.023>
- McGill, G. E., & Hills, L. S. (1992). Origin of giant Martian polygons. *Journal of Geophysical Research*, *97*(E2), 2633–2647. <https://doi.org/10.1029/91JE02863>
- McGill, R., Tukey, J. W., & Larsen, W. A. (1978). Variations of box plots. *The American Statistician*, *32*(1), 12–16.
- McGowan, E. M. (2009). Spatial distribution of putative water related features in southern Acidalia/Cydonia Mensae, Mars. *Icarus*, *202*, 78–89.
- Mellon, M. T., Arvidson, R. E., Marlow, J. J., Phillips, R. J., & Asphaug, E. (2008). Periglacial landforms at the Phoenix landing site and the northern plains of Mars. *Journal of Geophysical Research*, *113*, E00A23. <https://doi.org/10.1029/2007JE003039>
- Mellon, M. T., Feldman, W. C., & Prettyman, T. H. (2004). The presence and stability of ground ice in the southern hemisphere of Mars. *Icarus*, *169*(2), 324–340. <https://doi.org/10.1016/j.icarus.2003.10.022>
- Mellon, M. T., & Jakosky, B. M. (1995). The distribution and behavior of Martian ground ice during past and present epochs. *Journal of Geophysical Research*, *100*(E6), 11,781–11,799. <https://doi.org/10.1029/95JE01027>
- Milliken, R. E., Mustard, J. F., & Goldsby, D. L. (2003). Viscous flow features on the surface of Mars: Observations from high-resolution Mars orbiter camera (MOC) images. *Journal of Geophysical Research*, *108*(E6), 5057. <https://doi.org/10.1029/2002JE002005>
- Mitrofanov, I. G., Litvak, M. L., Kozyrev, A. S., Sanin, A. B., Tret'yakov, V. I., Grin'kov, V. Y., et al. (2004). Soil water content on Mars as estimated from neutron measurements by the HEND instrument onboard the 2001 Mars Odyssey spacecraft. *Solar System Research*, *38*, 253–265. <https://doi.org/10.1023/B:SOLS.0000037461.70809.45>
- Morgenstern, A., Hauber, E., Reiss, D., van Gasselt, S., Grosse, G., & Schirrmeyer, L. (2007). Deposition and degradation of a volatile-rich layer in utopia Planitia and implications for climate history on Mars. *Journal of Geophysical Research*, *112*, E06010. <https://doi.org/10.1029/2006JE002869>
- Moscardelli, L., Dooley, T., Dunlap, D., Jackson, M., & Wood, L. (2012). Deep-water polygonal fault systems as terrestrial analogs for large-scale Martian polygonal terrains. *GSA Today*, *22*(8), 4–9. <https://doi.org/10.1130/GSATG147A.1>
- Mouis, O., Chassefière, E., Lasue, J., Chevrier, V., Elwood Madden, M. E., Lakhilfi, A., et al. (2013). Volatile trapping in Martian clathrates. *Space Science Reviews*, *174*(1–4), 213–250. <https://doi.org/10.1007/s11214-012-9942-9>
- Mustard, J. F., Cooper, C. D., & Rifkin, M. K. (2001). Evidence for recent climate change on Mars from the identification of youthful near-surface ground ice. *Nature*, *412*, 411–414.
- Oehler, D. Z., & Allen, C. C. (2010). Evidence for pervasive mud volcanism in Acidalia Planitia, Mars. *Icarus*, *208*, 636–657.
- Oehler, D. Z., & Etiope, G. (2017). Methane seepage on Mars: Where to look and why. *Astrobiology*, *17*(12), 1233–1264. <https://doi.org/10.1089/ast.2017.1657>
- Orgel, C., Hauber, E., Skinner, Jr., J. A., van Gasselt, S., Ramsdale, J., Balme, M., et al. (2015). Distribution, origin and evolution of hypothesized mud volcanoes, thumbprint terrain and giant polygons in Acidalia, Utopia and Arcadia Planitiae: Implications for sedimentary processes in the northern lowlands of Mars. XLVI Lunar and Planetary Science Conference, Houston, TX, #1862.
- Page, D. P. (2018). A candidate methane-clathrate destabilisation event on Mars: A model for sub-millennial-scale climatic change on earth. *Gondwana Research*, *59*, 43–56. <https://doi.org/10.1016/j.gr.2018.03.010>
- Pathare, A. V., Feldman, W. C., Prettyman, T. H., & Maurice, S. (2018). Driven by excess? Climatic implications of new global mapping of near-surface water-equivalent hydrogen on Mars. *Icarus*, *301*, 97–116. <https://doi.org/10.1016/j.icarus.2017.09.031>
- Pelletier, J. D., Kolb, K. J., McEwen, A. S., & Kirk, R. L. (2008). Recent bright gully deposits on Mars: Wet or dry flow? *Geology*, *36*(3), 211–214. <https://doi.org/10.1130/G24346A.1>
- Pilorget, C., & Forget, F. (2016). Formation of gullies on Mars by debris flows triggered by CO₂ sublimation. *Nature Geoscience*, *9*(1), 65–69. <https://doi.org/10.1038/ngeo2619>
- Piqueux, S., Kleinböhl, A., Hayne, P. O., Heavens, N. G., Kass, D. M., McCleese, D. J., et al. (2016). Discovery of a widespread low-latitude diurnal CO₂ frost cycle on Mars. *Journal of Geophysical Research: Planets*, *121*, 1174–1189. <https://doi.org/10.1002/2016JE005034>

- Plaut, J. J., Safaeinili, A., Holt, J. W., Phillips, R. J., Head, J. W. III, Seu, R., et al. (2009). Radar evidence for ice in lobate debris aprons in the mid-northern latitudes of Mars. *Geophysical Research Letters*, *36*, L02203. <https://doi.org/10.1029/2008GL036379>
- Plescia, J. B. (1980). Cinder cones of Isidis and Elysium. *NASA Technical Memorandum*, 82385, 263–265.
- Prieto-Ballesteros, O., Kargel, J. S., Fairén, A. G., Fernández-Remolar, D. C., Dohm, J. M., & Amils, R. (2006). Interglacial clathrate destabilization on Mars: Possible contributing source of its atmospheric methane. *Geology*, *34*(3), 149–152. <https://doi.org/10.1130/G22311.1>
- Ramsdale, J. D., Balme, M. R., Conway, S. J., Gallagher, C., van Gasselt, S., Hauber, E., et al. (2017). Grid-based mapping: A method for rapidly determining the spatial distributions of small features over very large areas. *Planetary and Space Science*, *140*, 49–61. <https://doi.org/10.1016/j.pss.2017.04.002>
- Ramsdale, J. D., Balme, M. R., Gallagher, C., Conway, S. J., Smith, I., Hauber, E., et al. (2018). Gridmapping the northern plains of Mars: Geomorphological, Radar and Water-Equivalent Hydrogen results from Arcadia Planitia suggest possible fluvial and volcanic systems overlain by a ubiquitous and heavily degraded ice-rich latitude-dependent mantle. *Journal of Geophysical Research: Planets*, *123*. <https://doi.org/10.1029/2018JE005663>
- Reiss, D., Hiesinger, H., Hauber, E., & Gwinner, K. (2009). Regional differences in gully occurrence on Mars: A comparison between the Hale and Bond craters. *Planetary and Space Science*, *57*(8–9), 958–974. <https://doi.org/10.1016/j.pss.2008.09.008>
- Rice, J. W., & Edgett, K. S. (1997). Catastrophic flood sediments in Chryse Basin, Mars, and Quincy Basin, Washington: Application of sandar facies model. *Journal of Geophysical Research*, *102*(E2), 4185–4200. <https://doi.org/10.1029/96JE02824>
- Root, M. J., & Elwood Madden, M. E. (2012). Potential effects of obliquity change on gas hydrate stability zones on Mars. *Icarus*, *218*(1), 534–544. <https://doi.org/10.1016/j.icarus.2011.12.024>
- Salvatore, M. R., & Christensen, P. R. (2014). On the origin of the Vastitas borealis formation in Chryse and Acidalia Planitiae, Mars. *Journal of Geophysical Research: Planets*, *119*, 2437–2456. <https://doi.org/10.1002/2014JE004682>
- Schorghofer, N. (2008). Temperature response of Mars to Milankovitch cycles. *Geophysical Research Letters*, *35*, L18201. <https://doi.org/10.1029/2008GL034954>
- Schorghofer, N., & Aharonson, O. (2005). Stability and exchange of subsurface ice on Mars. *Journal of Geophysical Research*, *110*, E05003. <https://doi.org/10.1029/2004JE002350>
- Schorghofer, N., & Forget, F. (2012). History and anatomy of subsurface ice on Mars. *Icarus*, *220*, 1112–1120. <https://doi.org/10.1016/j.icarus.2012.07.003>
- Scott, D. H., & Tanaka, K. L. (1986). Geologic map of the western equatorial region of Mars: U.S. Geological Survey miscellaneous investigations series Map I–1802–A, scale 1:15,000,000.
- Seibert, N. M., & Kargel, J. S. (2001). Small scale Martian polygonal terrain: implications for liquid surface water. *Geophysical Research Letters*, *28*(5), 899–902. <https://doi.org/10.1029/2000GL012093>
- Séjourné, A., Costard, F., Gargani, J., Soare, R. J., Fedorov, A., & Marmo, C. (2011). Scalloped depressions and small-sized polygons in western utopia Planitia, Mars: A new formation hypothesis. *Planetary and Space Science*, *59*, 412–422.
- Séjourné, A., Costard, F., Gargani, J., Soare, R. J., & Marmo, C. (2012). Evidence of an eolian ice-rich and stratified permafrost in utopia Planitia, Mars. *Planetary and Space Science*, *60*(1), 248–254. <https://doi.org/10.1016/j.pss.2011.09.004>
- Séjourné, A., Costard, F., Swirad, Z. M., Losiak, A., Bouley, S., Smith, I., et al. (2018). Mapping the northern plains of Mars: using morphotype and distribution of ice-related landforms to understand multiple ice-rich deposits in Utopia Planitia. *Journal of Geophysical Research: Planets*, *123*. <https://doi.org/10.1029/2018JE005665>
- Seu, R., Biccari, D., Orosei, R., Lorenzoni, L. V., Phillips, R. J., Marinangeli, L., et al. (2004). SHARAD: The MRO 2005 shallow radar. *Planetary and Space Science*, *52*(1–3), 157–166. <https://doi.org/10.1016/j.pss.2003.08.024>
- Skinner, J. A. (2012). Constraining the origin of pitted cones in Chryse and Acidalia Planitiae, Mars, based on their statistical distributions and marginal relationships. 43rd Lunar and Planetary Science Conference, Houston, TX, Abstract #2905.
- Skinner, J. A., & Mazzini, A. (2009). Martian mud volcanism: Terrestrial analogs and implications for formational scenarios. *Marine and Petroleum Geology*, *26*, 1866–1878.
- Skinner, J. A., Tanaka, K. L., & Ferguson, R. L. (2008). Evidence for and implications of liquefaction in the Vastitas Borealis marginal unit in Southern Utopia Planitia, Mars. 39th Lunar and Planetary Science Conference, Houston, TX, Abstract #2418.
- Smith, D. E., Zuber, M. T., Frey, H. V., Garvin, J. B., Head, J. W., Muhleman, D. O., et al. (2001). Mars orbiter laser altimeter: Experiment summary after the first year of global mapping of Mars. *Journal of Geophysical Research*, *106*(E10), 23,689–23,722. <https://doi.org/10.1029/2000JE001364>
- Smith, I. B., & Holt, J. W. (2015). Spiral trough diversity on the north pole of Mars, as seen by shallow radar (SHARAD). *Journal of Geophysical Research: Planets*, *120*, 362–387. <https://doi.org/10.1002/2014JE004720>
- Smith, I. B., Putzig, N. E., Holt, J. W., & Phillips, R. J. (2016). An ice age recorded in the polar deposits of Mars. *Science*, *352*(6289), 1075–1078. <https://doi.org/10.1126/science.aad6968>
- Smith, M. J., Paron, P., & Griffiths, J. S. (2011). *Geomorphological mapping. Methods and applications* (p. 612). Amsterdam: Elsevier.
- Soare, R. J., Conway, S. J., & Dohm, J. M. (2014). Possible ice-wedge polygons and recent landscape modification by “wet” periglacial processes in and around the Argyre impact basin, Mars. *Icarus*, *233*, 214–228. <https://doi.org/10.1016/j.icarus.2014.01.034>
- Soare, R. J., Conway, S. J., Dohm, J. M., & El-Maarry, M. R. (2014). Possible open-system (hydraulic) pingos in and around the Argyre impact region of Mars. *Earth and Planetary Science Letters*, *398*, 25–36. <https://doi.org/10.1016/j.epsl.2014.04.044>
- Soare, R. J., Osinski, G. R., & Roehm, C. L. (2008). Thermokarst lakes and ponds on Mars in the very recent (late Amazonian) past. *Earth and Planetary Science Letters*, *272*(1–2), 382–393. <https://doi.org/10.1016/j.epsl.2008.05.010>
- Soare, R. J., Séjourné, A., Pearce, G. D., Costard, F., & Osinski, G. R. (2011). The Tuktoyaktuk coastlands of northern Canada: A possible wet periglacial analogue of Utopia Planitia, Mars. *Geological Society of America Special Papers*, *483*, 203–218. [https://doi.org/10.1130/2011.2483\(13\)](https://doi.org/10.1130/2011.2483(13))
- Soderblom, L. A., Kreidler, T. J., & Masursky, H. (1973). Latitudinal distribution of a debris mantle on the Martian surface. *Journal of Geophysical Research*, *78*(20), 4117–4122. <https://doi.org/10.1029/JB078i020p04117>
- Squyres, S. W. (1978). Martian fretted terrain: Flow of erosional debris. *Icarus*, *34*(3), 600–613. [https://doi.org/10.1016/0019-1035\(78\)90048-9](https://doi.org/10.1016/0019-1035(78)90048-9)
- Squyres, S. W. (1979). The distribution of lobate debris aprons and similar flows on Mars. *Journal of Geophysical Research*, *84*, 8087–8096.
- Stuurman, C. M., Osinski, G. R., Holt, J. W., Levy, J. S., Brothers, T. C., Kerrigan, M., et al. (2016). SHARAD detection and characterization of subsurface water ice deposits in Utopia Planitia, Mars. *Geophysical Research Letters*, *43*, 9484–9491. <https://doi.org/10.1002/2016GL070138>
- Tanaka, K. L., & Scott, D. H. (1987). Geologic map of the polar regions of Mars: U.S. Geological Survey miscellaneous investigations series Map I–1802–C, scale 1:15,000,000.

- Tanaka, K. L., Skinner, J. A., Dohm, J. M., Irwin, R. P. III, Kolb E. J., Fortezzo C. M., et al. (2014). Geologic map of Mars. U.S. Geological Survey Sci. Inv Map 3292.
- Tanaka, K. L., Skinner, J. A., Jr., & Hare, T. M. (2005). Geologic map of the northern plains of Mars: U.S. Geological Survey science investigations Map 2888, scale 1:15,000,000.
- Treiman, A. H. (2003). Geologic settings of Martian gullies: Implications for their origins. *Journal of Geophysical Research*, 108(E4), 8031. <https://doi.org/10.1029/2002JE001900>
- Ulrich, M., Hauber, E., Herzsuh, U., Härtel, S., & Schirrmeyer, L. (2011). Polygon pattern geomorphometry on Svalbard (Norway) and western Utopia Planitia (Mars) using high-resolution stereo remote-sensing data. *Geomorphology*, 134(3-4), 197–216. <https://doi.org/10.1016/j.geomorph.2011.07.002>
- Ulrich, M., Morgenstern, A., Günther, F., Reiss, D., Bauch, K. E., Hauber, E., et al. (2010). Thermokarst in Siberian ice-rich permafrost: Comparison to asymmetric scalloped depressions on Mars. *Journal of Geophysical Research*, 115, E10009. <https://doi.org/10.1029/2010JE003640>
- van Gasselt, S., Hauber, E., & Neukum, G. (2010). Lineated valley fill at the Martian dichotomy boundary: Nature and history of degradation. *Journal of Geophysical Research*, 115, E08003. <https://doi.org/10.1029/2009JE003336>
- Vincendon, M. (2015). Identification of Mars gully activity types associated with ice composition. *Journal of Geophysical Research: Planets*, 120, 1859–1879. <https://doi.org/10.1002/2015JE004909>
- Vincendon, M., Mustard, J., Forget, F., Kreslavsky, M., Spiga, A., Murchie, S., et al. (2010). Near-tropical subsurface ice on Mars. *Geophysical Research Letters*, 37, L01202. <https://doi.org/10.1029/2009GL041426>
- Viola, D., McEwen, A. S., Dundas, C. M., & Byrne, S. (2015). Expanded secondary craters in the Arcadia Planitia region, Mars: Evidence for tens of Myr-old shallow subsurface ice. *Icarus*, 248, 190–204. <https://doi.org/10.1016/j.icarus.2014.10.032>
- Viola, D., McEwen, A. S., Dundas, C. M., & Byrne, S. (2017). Subsurface volatile content of martian double-layer ejecta (DLE) craters. *Icarus*, 284, 325–343. <https://doi.org/10.1016/j.icarus.2016.11.031>
- Voelker, M., Hauber, E., Schulzeck, F., & Jaumann, R. (2017). Grid-mapping Hellas Planitia, Mars – Insights into distribution, evolution and geomorphology of (Peri)-glacial, fluvial and lacustrine landforms in Mars' deepest basin. *Planetary and Space Science*, 145, 49–70. <https://doi.org/10.1016/j.pss.2017.07.012>
- Webster, C. R., Mahaffy, P. R., Atreya, S. K., Moores, J. E., Flesch, G. J., Malespin, C., et al. (2018). Background levels of methane in Mars' atmosphere show strong seasonal variations. *Science*, 360(6393), 1093–1096. <https://doi.org/10.1126/science.aaq0131>
- Weitz, N., Zanetti, M., Osinski, G. R., & Fastook, J. L. (2018). Modeling concentric crater fill in utopia Planitia, Mars, with an ice flow line model. *Icarus*, 308, 209–220. <https://doi.org/10.1016/j.icarus.2017.08.023>
- Werner, S. C., Tanaka, K. L., & Skinner, J. A. (2011). Mars: The evolutionary history of the northern lowlands based on crater counting and geologic mapping. *Planetary and Space Science*, 59(11-12), 1143–1165. <https://doi.org/10.1016/j.pss.2011.03.022>
- Wilhelms, D. E. (1990). Geologic mapping. In R. Greeley & R. M. Batson (Eds.), *Planetary Mapping* (pp. 208–260). New York: Cambridge University Press.
- Willmes, M., Reiss, R., Hiesinger, H., & Zanetti, M. (2012). Surface age of the ice–dust mantle deposit in Malea Planum, Mars. *Planetary and Space Science*, 60(1), 199–206. <https://doi.org/10.1016/j.pss.2011.08.006>
- Wilson, J. T., Eke, V. R., Massey, R. J., Elphic, R. C., Feldman, W. C., Maurice, S., et al. (2018). Equatorial locations of water on Mars: Improved resolution maps based on Mars odyssey neutron spectrometer data. *Icarus*, 299, 148–160. <https://doi.org/10.1016/j.icarus.2017.07.028>
- Wu, Z., Barosh, P. J., Hu, D., Wu, Z., Peisheng, Y., Qisheng, L., et al. (2005). Migrating pingos in the permafrost region of the Tibetan plateau, China and their hazard along the Golmud-Lhasa railway. *Engineering Geology*, 79(3-4), 267–287. <https://doi.org/10.1016/j.enggeo.2005.02.003>
- Zanetti, M., Hiesinger, H., Reiss, D., Hauber, E., & Neukum, G. (2010). Distribution and evolution of scalloped terrain in the southern hemisphere, Mars. *Icarus*, 206(2), 691–706. <https://doi.org/10.1016/j.icarus.2009.09.010>